RESEARCH ON THE NOISE PRODUCED BY LARGE SCALE STRUCTURE IN SUPERSONIC JETS

GRANT NO. NAG-1-159

FINAL REPORT TO

NASA LANGLEY RESEARCH CENTER

Period: March 1, 1981 to June 30, 1982

By

Dennis K. McLaughlin
Dynamics Technology, Inc.

and

David G. Lilley
Oklahoma State University

Principal Investigators

NASA Technical Officer: Dr. J. M. Seiner
Acoustic and Noise Reduction Division

NASA Grants Officer: Mr. C. L. Crowder

RESEARCH ON THE NOISE PRODUCED BY LARGE SCALE STRUCTURE IN SUPERSONIC JETS

GRANT NO. NAG-1-159

FINAL REPORT TO

NASA LANGLEY RESEARCH CENTER

Period: March 1, 1981 to June 30, 1982

By

Dennis K. McLaughlin
Dynamics Technology, Inc.

and

David G. Lilley
Oklahoma State University

Principal Investigators

NASA Technical Officer: Dr. J. M. Seiner
Acoustic and Noise Reduction Division

NASA Grants Officer: Mr. C. L. Crowder

TABLE OF CONTENTS

I. FOREWORD

This constitutes the final report on the project entitled "Research on the Noise Produced by Large Scale Structure in Supersonic Jets." The research was supported by NASA Langley Research Center under Grant Number NAG-1-159 to Oklahoma State University. The project was initiated with Dr. Dennis K. McLaughlin as Principal Investigator. In August 1981, Dr. McLaughlin joined Dynamics Technology, Inc. in Torrance, California. He continued to supervise the research of graduate students T. F. Hu and M. D. Politte during the next year. This supervision was conducted through subcontract No. 8179 to Dynamics Technology. Professor David G. Lilley of Oklahoma State University became a Principal Investigator in August 1981 to assist in the supervision of the graduate students.

A major part of this final report are the reports prepared by Mark D. Politte and Lee-Fen Ko under the supervision of Dr. McLaughlin. The Ph.D. Dissertation of Dr. T. F. Hu also reports on research conducted with NASA support and has been submitted previously under separate cover.

II. TECHNICAL SUMMARY

Experiments and computations on the flowfield and radiated noise of supersonic jets were undertaken in this research program. Both aspects were directed towards understanding the noise production mechanisms associated with the large scale structure in supersonic jets.

There were two major activities in the experimental program. First, flowfield and acoustic measurements were performed on a perfectly expanded Mach number 2.1 jet. These measurements explored the effect of several exit conditions on the development of a moderate Reynolds number supersonic jet. The experiments were conducted using a new dual-electrode glow discharge device in which two electrodes were placed on opposite sides of the jet nozzle, near the exit plane. Sinusoidal signals, both in-phase and out-of-phase, applied to these electrodes preferentially excited the $n = 0$ (varicose) and the $n = \pm 1$ (helical) modes of instability, respectively. The relative strength of these large scale instability modes in radiating noise was evaluated.

In addition to the dual glow excitation, the effect of roughening the exiting nozzle boundary layer was evaluated. It was shown that the exiting shear layer contained fluctuations of broader band frequency content than the natural jet case. These measurements provided a valuable comparison to measurements performed in a conventional high Reynolds number model jet at NASA Langley Research Center using a hot-film probe.

The second major activity in the experimental program consisted of a study of shock associated noise in a low to moderate Reynolds number jet begun under the previous year's NASA Grant No. 1-10. In this study, significant broadband shock-associated noise was identified and measured in the moderate Reynolds number supersonic jet. The low Reynolds number under-expanded supersonic jets produce very little broadband shock associated noise. However, many of the flowfield fluctuation properties associated with shock 'screech' were measured and quantified (at the low Reynolds number condition).

In the computational program, calculations were performed of noise radiated from experimentally measured instabilities in moderate and high Reynolds number supersonic jets using the computer code LSNOIS. It was shown that the evolution of the relative phase of the dominant spectral component is as important, or more important, than the evolution of the amplitude. Inclusion of both the experimental amplitude and phase distributions in the LSNOIS computer calculation produces a calculated near field that is very close to that experimentally measured. Finally, the problem of numerical oscillations in the near field sound calculations using LSNOIS has been determined to be caused by an improper choice of the axial step size. Changing the axial mesh reduces the problem of numerical oscillations. These calculations have continued to demonstrate the very promising capability of the noise prediction method involving large scale instability computations.

III. SUMMARY OF PUBLICATIONS

A. STUDENTS' REPORTS AND DISSERTATIONS:

1) "Experiments on Model Jets With Dual Electrode Glow Discharge Excitation," M.S. Report by Mark D. Politte, May 1982.

2) "An Evaluation of the Noise Radiation Calculation of the Computer Code LSNOIS," M.S. Report by Lee-Fen Ko, May 1981.

3) "Flow and Acoustic Properties of Low Reynolds Number Under-expanded Supersonic Jets," Ph.D. Dissertation by T. F. Hu, December 1981.

B. PUBLICATIONS IN PREPARATION FOR THE OPEN LITERATURE:

Several manuscripts are in preparation for submission to technical journals based upon this research. Copies of these papers will be forwarded to the NASA Technical Officer when they become available.

Attachment #1

EXPERIMENTS ON MODEL JETS WITH DUAL ELECTRODE GLOW DISCHARGE EXCITATION

M.S. Report

by

Mark D. Politte

EXPERIMENTS ON MODEL JETS WITH DUAL ELECTRODE GLOW DISCHARGE EXCITATION

By

MARK D. POLITTE

Bachelor of Science
Oklahoma State University
Stillwater, Oklahoma
1980

Submitted to the Faculty of the
Mechanical and Aerospace
Engineering Department of the
Oklahoma State University
in partial fulfillment of
the requirements for
the degree of
MASTER OF SCIENCE
May, 1982

ACKNOWLEDGEMENTS

The author wishes to express his appreciation to Dr. Dennis K. McLaughlin for his helpful advice concerning this study, and to his committee members, Dr. D. G. Lilley, Dr. P. M. Moretti, and Dr. A. J. Ghajar for their guidance.

Appreciation is extended to Dr. Tieh Feng Hu for his helpful comments.

The author would also like to express his gratitude toward his wife, Sue, for her assistance in typing, preparing the figures, and general support.

Finally, the author would like to recognize the financial support of the National Aeronautics and Space Administration.

ABSTRACT

Using a dual electrode glow discharge excitation device, a method of mode selection into either the n = 0 or n = $\pm$1 azimuthal modes has been developed and tested by Fourier analyzing experimental azimuthal phase and amplitude data. On a M = 2.1 moderate Reynolds number (Re = 68,000) jet with a laminar boundary layer, under n = 0 or n = $\pm$1 excitation, coherent axial wave evolution, mean flow, and sound pressure level directivity measurements have been performed. The boundary layer of this same jet has been excited using a grit coating on the nozzle wall, and bandpassed axial wave evolution data obtained and compared to the measurements made by previous workers on a conventional high Reynolds number jet (Re = 5×10^6) using a hot-film type probe.

Good agreement exists between the coherent wave evolution data obtained in this study, and a computer prediction based on instability wave theory. The n = $\pm$1 mode was found to be the preferred mode of the jet, but the n = 0 mode was found to be a more effective noise producer at the M = 2.1, Re = 68,000 condition. The glow discharge method could not be used with the excited boundary layer nozzle. The bandpassed axial wave evolution data obtained on the excited boundary layer jet compared qualitatively with the M = 2.0, Re = 5×10^6 data, and helps to establish the validity of the hot-film probe technique in high Reynolds number supersonic jet flows.

TABLE OF CONTENTS

LIST OF FIGURES

NOMENCLATURE

A_m	mass velocity fluctuation sensitivity coefficient
A_T	stagnation temperature fluctuation sensitivity coefficient
D	nozzle exit diameter
e	hot-wire voltage
f	frequency (Hz)
M	Mach number
n	azimuthal mode number
P	pressure
P_{atm}	standard atmospheric pressure
P_{ch}	test chamber pressure
P_e	static nozzle exit pressure
P_o	stagnation pressure
r	radial distance from jet centerline, cylindrical coordinate system
r(.5)	radial location where u = 0.5U
R	radial distance from center of jet at nozzle exit, spherical coordinate system
Re	Reynolds number $\frac{U_o D}{\nu}$
St	Strouhal number, fD/U_o
T	temperature
$\bar{u}$	local mean velocity
U	local jet centerline velocity

U_o	jet centerline exit velocity
x	downstream distance from the nozzle
y	vertical distance from the centerline
z	horizontal distance from the centerline
β	angular coordinate in spherical coordinate system, measured from x axis
δ	local shear layer thickness
η	$\frac{r - r(.5)}{\delta}$
θ	azimuthal angle
ν	kinematic viscosity
ρ	density
τ	period of the organized wave
ϕ	relative sensor phase angle
$( )_t$	quantity evaluated at stagnation conditions
$( )_o$	quantity evaluated at jet exit
$( )_{max}$	quantity evaluated at location of maximum amplitude
$\overline{( )}$	time average of quantity
$( )_{rms}$	root mean square of quantity
	phase average of quantity
$( )'$	total fluctuation, $( )' = ( ) + ( )''$
$( )''$	random portion of fluctuation
$( )$	periodic portion of fluctuation

CHAPTER I

INTRODUCTION

A. Perspectives

It has become evident due to the research efforts of many workers during the past ten years that large scale coherent flow fluctuations are present in supersonic turbulent jets. The most recent aerodynamic noise theories, such as that developed by Morris and Tam (1), start with the governing equations of fluid dynamics and model flow fluctuations using instability wave theory.

Research conducted at Oklahoma State University on low Reynolds number ($Re \approx 8{,}000$) jets which are laminar for large distances downstream have provided valuable data, relatively free of the complications of turbulence, for checking the instability wave theory. In fact good agreement between theory and experiment has been shown to exist, as shown in Figure 1, (3). However, a low Reynolds number jet is not a good model of a conventional high Reynolds number jet ($Re \approx 10^6$) exhausting into atmospheric pressure, which possesses a turbulent shear layer.

It is often assumed that in supersonic jets the large scale flow instabilities can be well represented by a superposition of the axisymmetric ($n = 0$), and antisym-

metric (n = $\pm$1) azimuthal modes. Sketches of the wavefronts of the n = 0 mode and n = $\pm$1 modes are shown in Figure 2, and instantaneous stream lines of the jet of the two modes are shown in Figure 3. However, in a natural jet it is extremely difficult to measure the downstream evolution of a coherent instability wave due to the difficulty in obtaining a phase reference. At Oklahoma State University a technique using a glow discharge has been used to preferentially excite a spectral component of the flow, and to provide the needed upstream reference. With this technique, using a single exciter, Troutt (4) has been successful in exciting a combination of n = 0 and n = $\pm$1 modes, with the relative proportions of the modes dependent upon the frequency of excitation. A method of mode selection which would preferentially excite only the n = 0 or n = $\pm$1 modes would provide useful data for a more stringent check of the instability wave theory, and might also be helpful in determining the mode preference of the jet, and also the relative effectiveness of the modes in the production of radiated noise.

Troutt (4) performed his measurements on a moderate Reynolds number (Re $\approx$ 68,000) jet which had an exiting laminar boundary layer, that underwent transition to a turbulent shear layer over the first two or three jet diameters. When his mean flow results were used as input to the Morris-Tam instability theory (documented in Tester, et al (5)) and the output checked against his axial co-

herent wave evolution data, quite good agreement was obtained (3). See Figure 4. Although the jet used by Troutt was an improvement over the low Reynolds number jet as a model of a conventional high Reynolds number flow ($Re \approx 10^6$), it still had an exiting laminar shear layer which takes one to three diameters to develop to a turbulent shear layer. Therefore, this jet is not a totally accurate representation of a conventional jet whose shear layer is almost immediately turbulent from its inception.

McLaughlin, Seiner, and Liu (3) performed experiments on a jet of Reynolds number ($Re \approx 5 \times 10^6$) which had a turbulent shear layer almost immediately upon exit. However, since they had not devised an excitation mechanism allowing coherent wave evolution data to be obtained, they used fluctuations in a specific bandpass to approximate the wave amplitude evolution data. The present instability theory models the coherent portion of the wave. The approximation in using bandpassed data could explain the poorer agreement obtained between experiment and prediction (Figure 5).

A moderate Reynolds number jet which had an exiting turbulent shear layer and a laminar core would be a closer approximation to a conventional jet than the jet used by Troutt, and would allow the use of delicate hot-wire probes, used previously at Oklahoma State, to obtain axial wave evolution data. The low pressures associated

with the moderate Reynolds number would presumably allow the use of our present glow discharge technique, and coherent axial wave evolution data could be obtained, which would provide a stringent test of the theoretical calculation.

B. Goals and Objectives

With the above in mind, the major goal of this research has been to increase the data base for checking the increasingly complex wave instability theory, and to interpret these data to try to explain the physical behavior of the jet under various excitation conditions. The first set of objectives in this study deal with measurements performed on a moderate Reynolds number jet with an exiting laminar boundary layer. They are as follows:

1. To demonstrate that preferential mode separation into either $n = 0$ or $n = \pm 1$ modes is possible using a dual exciter technique, and to determine the success of mode separation.
2. To perform mean flow measurements in the $n = 0$ and $n = \pm 1$ modes to provide data for use as input to the instability model computation.
3. To obtain axial coherent wave evolution data in the $n = 0$ and $n = \pm 1$ cases to check the results of the theoretical calculation.
4. To try to determine which mode is the preferred mode, or more likely to occur in a natural un-

excited jet, and to determine the relative effectiveness of the modes in the production of radiated noise.

The second set of objectives deal with measurements performed on a moderate Reynolds number jet with an exiting turbulent shear layer. They are as follows:

1. To first excite the boundary layer in the nozzle and establish that the flow is indeed turbulent in the shear layer close to the nozzle exit, but approximately laminar on the centerline of the jet.
2. To perform axial wave evolution measurements on the jet with no glow excitation, to check the results of McLaughlin, Seiner, and Liu (3), who used a wedge type hot film probe.
3. To obtain axial coherent wave evolution data utilizing the glow exciter as in (3) above.

CHAPTER II

EXPERIMENTAL APPARATUS

A. General Facility

The experiments were performed in the Oklahoma State University high speed jet noise facility, shown schematically in Figure 6. High pressure air is supplied by a Worthington compressor, dried by a chemical dessicant, and stored in a 1.8 cubic meter spherical pressure vessel. Enough air can be stored to allow continuous operation of the facility for several hours without running the compressor. The upstream pressure is kept constant by a regulator, followed by a throttling valve, a stilling section, and a contraction section (area ratio 325:1). The stilling section is 55 cm long with a 14.3 cm inside diameter, consisting of five cm of foam, three perforated plates, a 7.6 cm honeycomb section, and six fine mesh screens. The contraction section with a cubic contour matches the stilling section nozzle.

The nozzle used for all measurements was designed using the method of characteristics, with an inviscid design Mach number of 2.0 and an exit diameter of 10 mm. The nozzle contour also included a boundary layer corr-

ection, made at a Reynolds number of 20,000, since the nozzle was intended for use at higher and lower Reynolds numbers.

The nozzle exhausts into a 114 cm x 76 cm x 71 cm test chamber lined with 5 cm of acoustic foam. The static pressure within the chamber was controlled by evacuating the air through a variable throat diffuser with a 0.01 m^3/s Kinney vacuum pump, with the pressure fluctuations of the pump dampened by isolating the pump from the test chamber with a 30 cubic meter storage tank.

The test chamber is equipped with a probe drive capable of translation in three orthogonal directions, and by means of various adapters able to facilitate the use of hot-wire probes, pitot or static pressure probes, and microphones. Precision ten-turn potentiometers provide the probe drive system with constant DC voltages proportional to the probe location. The coordinate system used for the measurements is shown in Figure 7.

A dual glow discharge device employed in the experiments is very similar to the single glow exciter used previously at Oklahoma State University (2, 4). 1.02 mm tungsten electrodes insulated by ceramic tubing, fitted in brass sleeves, were mounted on the nozzle so that the tips of the electrodes were flush with the inner nozzle surface, and about 2 mm from the nozzle exit. The electrodes were mounted so that they were 180^{o} apart from each other in azimuthal angle (Figure 7). When operated at low pressure,

the electrodes produce an oscillating glow (ionization of the air) when subjected to an alternating voltage (700 V p to p) biased to a 400 V DC negative potential. Matched electrical components were used in each individual circuit to ensure as much as possible that the glows were identical. One circuit was equipped with an inverter so that it could be operated in phase or 180^{o} out of phase with the other glow.

B. Instrumentation

Pressure measurements were made with a mercury manometer referenced to a vacuum of 30 micrometers of Hg. Pressure taps were located in the flow contraction area just upstream of the nozzle, near the exit of the nozzle, and near the top of the chamber for measuring stagnation pressure P_o, exit pressure P_e, and chamber pressure P_{ch} respectively.

A pitot probe shown in Figure 8, consisting of a 0.53 mm OD tube with a flat end cut perpendicular to the tube axis was used in this study. A Statham PL96TCd-3-550 strain gage type transducer converted the pressure sensed by the probe into an electrical signal, which was converted into digital readout by a Vishay VE-20 strain indicator.

The normal hot-wire probes used in this study were DISA 55A53 subminature probes mounted on brass wedges, as shown in Figure 9. The associated constant temperature anemometry electronics consisted of a DISA 55M01 main

frame with a 55M10 standard bridge. The frequency response of the hot-wire and electronics was at least 60 kHz based on square wave response tests.

A Bruel and Kjaer 3175 mm diameter type 4138 condenser midrophone was used for the acoustic measurements. Based on factory specifications, the microphone was assumed to have onmi-directional response $\pm$3 dB for frequencies up to 60 kHz. Calibration of the microphones was performed with a B & K type 4220 piston phone. Associated microphone electronics included a B & K type 2618 preamplifier and a B & K type 2804 power supply.

Frequency spectra of the hot wire signals were made using a Tektronix 7L5 spectrum analyzer, and recorded with a Tektronix C-59 oscilliscope camera. A Saicor SAI 43A correlation and probability analyzer was used for correlating and phase averaging hot-wire and microphone signals.

CHAPTER III

EXPERIMENTAL PROCEDURES

A. General

All experiments were performed on the jet in as close to perfectly expanded conditions as possible, with the chamber pressure controlled to be within 3% of the nozzle exit pressure. The jet stagnation temperature was room temperature (294 K), and the Reynolds number based on exit conditions was approximately 68,000.

The microphone signals were high pass filtered at 2 kHz to eliminate the portion of the signal due to a test chamber resonance at about 500 Hz. The signal was also low passed filtered at 60 kHz to eliminate the portion of the signal due to a resonance which occurs at 100 kHz with this type of microphone in low pressure enviroments. For consistency, the fluctuating portion of the hot-wire signal was high and low pass filtered at the same frequencies as the microphone signal.

B. Cross Correlation and Phase Averaging

The oscillating glow discharge device was used to initiate a periodic disturbance into the flow and to pro-

vide a time and phase reference. The rms power output of the glow was calculated to be less than 2×10^{-3} of the total energy flux of the jet.

In the correlation mode, the Saicor analyzer was used to measure the phase lag between the signal sensed by the probe and the glow exciter. In the exhance mode, the analyzer was used to phase average the probe signal with the exciter signal used as a time reference. The phase averaged signal is mathematically expressed as

$$\langle f(t) \rangle = \lim_{N \to \infty} \frac{1}{N} \sum_{n=0}^{N} f(t + n\tau)$$

where τ is the period of the coherent disturbance, n is the number of disturbance cycles averaged over, and t is time. Application of this function allows the recovery of the periodic portion $\tilde{f}(t)$ of the fluctuation signal generated by the glow exciter, where the total signal generated is

$$f(t) = \bar{f} + \tilde{f}(t) + f''(t)$$

where $\bar{f}$ represents the mean component and f''(t) is the random turbulent contribution.

C. Hot-Wire Data Analysis

In supersonic flow fluctuation measurements, the instantaneous hot-wire bridge voltage e' can be represented by the following expression (6):

$$\frac{e'}{\bar{e}} = Am \frac{(\rho u)'}{\overline{\rho u}} + A_T \frac{T_t'}{\overline{T_t}}$$

Troutt (4) has shown that the stagnation temperature fluctuations under the flow conditions in this study are negligible, which means the hot-wire voltage fluctuations are proportional only to the mass velocity fluctuations. The proportionality factor Am was determined from direct calibration in the mean flow of the jet for each individual hot-wire, where

$$Am = \frac{\partial \ln \bar{e}}{\partial \ln \overline{\rho u}} \Bigg]_{T_w,\ T_t}$$

D. Acoustic Measurements

Since acoustic measurements were performed in a low density environment, the reference pressure used to calculate the standard sound pressure level (SPL) in dB was scaled by the ratio of the test chamber pressure to standard atmospheric pressure. The equation used to calculate SPL is given by

$$SPL = 20 \log_{10} \frac{(p')rms}{2 \times 10^{-5} (P_{ch}/P_{atm})}$$

with pressure given in N/m^2.

CHAPTER IV

EXPERIMENTAL RESULTS

A. Laminar Boundary Layer Jet

A.1. Acoustic Azimuthal Phase and Amplitude Measurements

In past work at Oklahoma State University, attempts were made to measure the phase and amplitude of the disturbances around the azimuth of the jet initiated by a single glow discharge, using a hot-wire probe in the shear layer (7, 8). However, probe resolution problems were encountered due to the variation of the phase of the disturbance with radial position. To solve this problem, azimuthal measurements were made in the near acoustic field with a microphone, on the assumption that the pressure disturbances in the near acoustic field (well out of the flow, however) accurately represent the flow fluctuation content (9).

As mentioned previously, Troutt (4), using a single glow exciter was able to excite both the $n = 0$ mode and $n = \pm 1$ modes, the relative amount of each mode depending upon the frequency of excitation. Figures 10 and 11 show Troutt's results for measurements made at $x/D = 12$ and $r/D = 3$ for Strouhal numbers of 0.20 and 0.38, respec-

tively. He deduced the ratio of n = 0 mode to n = ± 1 mode (A_o/A_1) for the St = 0.19 disturbance to be equal to 1.4, and for the St = 0.38 disturbance to be equal to 0.5.

In this study, a repeat of the single glow exciter measurement for the St = 0.38 component resulted in an A_o/A_1 ratio of approximately 1.55 when Fourier analyzed using the method developed by Hu (10). Figures 12 and 13 show the results of the measurement made at x/D = 11 and r/D = 4 and of Hu's azimuthal analysis program AZIMUS. The difference in modal composition is probably due to a combination of differences in excitation level and in probe location.

Since the n = 0 mode is axisymmetric (Figure 2), it seemed plausible that excitation with two glows, separated by 180 degrees in azimuth and firing simultaneously, would tend to excite preferentially the n = 0 mode. The effect on the flow of such excitation would be such that the flow fluctuations, and hence the near field acoustic radiation, would be axisymmetric around the azimuth of the jet. This implies that both the relative phase of the flow fluctuations, with respect to the excitation, and the amplitude of the fluctuations, should not change with azimuthal angle. Examination of Figure 14, showing the results of measurements made at x/D = 12 and r/D = 3 for St = 0.20 excitation with the glows in phase, shows that pure n = 0 mode behavior is very closely approximated. A modal decomposition of this data using AZIMUS is shown in Figure 15, and

confirms the fact that the n = 0 mode is definitely predominate under axisymmetric excitation conditions.

The purely antisymmetric instability mode is composed of equal amounts of n = 1 and n = -1 modes, whose wavefronts appear as helicies spiraling in opposite directions. When these helical wavefronts are superimposed, the effect on the mean flow of the jet is an oscillation or "flapping" of the jet, with no preferred plane of oscillation in a natural jet.

If the same dual glow exciter as described previously, firing 180^{o} out of phase, was able to preferentially excite only the n = ± 1 mode, the jet should oscillate in the vertical plane, and the flow fluctuations of the jet should maximize at azimuthal positions of 0^{o} and 180^{o}, and be equal to zero at 90^{o} and 270^{o}. At the sides of the jet (azimuthal positions of 90^{o} and 270^{o}), the phase should experience a discontinuity measured relative to the top glow for pure n = ± 1 mode excitation.

Figure 16 shows the results of the measurements of the azimuthal distribution of the phase and amplitude of the near acoustic field (x/D = 12, r/D = 3), at a frequency of excitation St = 0.20 with the glows out of phase. From this figure it can be seen that the response of the jet is close to that characteristic of pure n = ± 1 mode excitation, but it is clear that there are other modes present. Figure 17 shows the results of the modal decomposition, and from this figure the ratio A_1/A_o is approxi-

mately equal to 3.3 with the n = +1 and n = -1 modes present in approximately equal amounts. Although the mode separation in the out of phase case is not as good as with the glows in phase, it is still a good technique for achieving a flow where the n = $\pm$1 mode is largely predominant.

A.2. Mean Flow Results

Velocity profiles in the y and z planes were calculated using isentropic flow relations for data obtained from pitot probe measurements, and by assuming that the static pressure in the shear layer is equal to the test chamber pressure (3). The velocity profiles were fit to a half Gaussian curve of the form

$$\frac{\bar{u}}{U} = \exp[-2.773(\eta + 0.5)^2] \qquad \text{for } \eta > -0.5$$

$$= 1 \qquad \text{for } \eta \leq -0.5$$

where $\eta = \frac{r - r(.5)}{\delta}$, $\bar{u}$ is the local mean velocity, U is the local centerline velocity, δ is the local shear layer thickness, and r(.5) is the radial location where the mean velocity is 0.5U. Downstream of the potential core, $\delta = 2r(.5)$ and η reduces to $\eta = \frac{r}{\delta} - \frac{1}{2}$, where δ is now 1/2 the local jet diameter. The local jet diameter is defined as the locus of points where the mean velocity is 0.01 times the local centerline velocity.

The use of this curve fit for supersonic jets was first used by McLaughlin et al. (3) for a conventional

high Reynolds number jet, and then later shown to be useful in parameterizing the velocity profile data of moderate Reynolds number jets by Troutt and McLaughlin (9). The computer code used in this study (PITOT) was developed by another graduate student at O. S. U. and requires Tektronics graphics capability. Documentation is available from the Mechanical and Aerospace Engineering Department of Oklahoma State University.

Since the glows are point exciters, the effect of the excitation on the mean flow is more predominant in the vertical shear layers. Figures 18 and 19 show the values of the r(.5) and δ parameters used to generate the best curve fits for the average of measurements made in the bottom and side shear layers, for in phase and out of phase excitation at St = 0.20. The figures show that the double glow in both the in phase and out of phase case enhances the development of the mean flow, and shortens the length of the potential core, as noted by Troutt (8) in single glow excitation. In phase excitation tends to thicken the shear layer of the jet slightly more than the out of phase case.

A.3. Flow Fluctuation Results

In all flow fluctuation measurements, the response of the jet was found to be very sensitive to the frequency of excitation. The qualitative nature of the results varied from day to day, as the jet seemed to respond more

to excitation on some days than on others. The surface condition of the tungsten electrode was a factor, since toward the end of an experiment it deterioriated due to the locally high temperature, resulting in higher surface resistance. Although the DC current level was maintained by adjusting the DC bias voltage, the impedance matching of the AC power source and transformer precluded accurately keeping the AC current constant as the resistance of the glow tip increased. Despite all this, the qualitative aspects of the results were repeatable.

Figure 20 shows the results of axial wave evolution measurements for the in phase case at St = 0.23. The measurement location for these data and all subsequent shear layer measurements was in the shear layer at the position of maximum band passed hot-wire fluctuation voltage. The rms mass-velocity fluctuations are non-dimensionalized with respect to the mean exit mass-velocity on the centerline $(\overline{\rho u})_o$. The total and coherent fluctuation levels peak at x/D = 5, and the coherent portion of the fluctuations decays much faster than the overall fluctuation amplitude. Figure 21 shows the results of similar measurements made on the jet centerline for in phase excitation. Compared with the shear layer measurements, the coherent fluctuation amplitude remains a larger fraction of the total fluctuations as the disturbances travel downstream.

The results of measurements made in the shear layer of the jet excited with the glows out of phase at St = 0.22

is shown in Figure 22. The fluctuation levels peak at x/D = 6, and the overall fluctuation amplitude decays almost equally with the coherent portion. Examination of Figures 20 and 22 shows that the n = 0 mode produces a lower peak coherent wave amplitude than the n = $\pm$1 mode.

One of the major results of this study involves the measurements of the instability wave evolutions of the St = 0.23 phase averaged component in the excited jet using both in phase and out of phase electrode excitation. The ability to separate the modes by this type of excitation allows a direct comparison to be made with the instability theory calculation. When the n = 0 mode centerline hot-wire data are compared to a computer prediction based on the previously mentioned Morris-Tam algorithm, reasonable agreement is obtained, as shown in Figure 23, particularly for the decay portion of the curve. The mean flow data used as input to the computer code was that obtained by Troutt and Mclaughlin (9) on the same jet using a single glow at St = 0.20. This was done because the mean flow of a jet excited with a dual electrode exciter is almost identical to that excited with a single glow.

Figure 24 shows the n = $\pm$1 mode coherent amplitude data compared to the computer prediction. The agreement is excellent in both the growth and decay regions. In this comparison measurements performed in the shear layer are compared with the prediction since on the centerline

the n = $\pm$1 mode is negligible (until the end of the potential core). The very good agreement between prediction and experiment for the evolution of both the n = 0 and n = $\pm$1 modes suggest that the analysis is modelling the major components of the physics.

A.4. Acoustic Sound Pressure Level Measurements

Sound pressure level (SPL) directivity measurements, made at an arc radius of 30 jet diameters, were performed for the in phase and out of phase excitation cases at St = 0.22. The arc was centered at x/D = 6, since this was the approximate location where the flow fluctuations peaked. Coherent SPL is shown in Figure 25, and overall SPL in Figure 26. The n = 0 mode can be seen to produce higher coherent and overall noise levels for angles of 50^{o} or less. It is important to mention at this point that when the measurements at each angle were made, they were made during the same experimental run, the only difference being the setting of the switch used to control the signal inversion to one glow. In other words, the results are reliable in their qualitative nature. It is an apparent anomaly that the n = $\pm$1 mode, which has higher coherent and overall shear layer flow fluctuations, would produce less noise that the n = 0 mode, but under the experimental conditions of this study, that appears to be the case.

Hu (10), using the same glow discharge techniques

used in this study, found the n = $\pm$1 mode to produce higher coherent sound pressure levels than the n = 0 mode in an underexpanded M = 1.4 low Reynolds number jet excited at St = 0.37, the data shown in Figure 27. He found the overall SPL to be about the same, regardless of the mode of excitation. Hu's results are mentioned only to point out that the effect of the various modes on the noise production of the jet is not a well understood phenomenon, and that further work in this area is needed.

B. Excited Boundary Layer Jet

B.1. Preliminary Measurements

The goal of this portion of the research was to obtain a turbulent shear layer at the exit of the jet, and still retain a jet core which contained relatively low flow fluctuation content compared to the shear layer. To do this required that only the boundary layer of the nozzle be tripped or altered. Before attempting this, for comparison purposes hot-wire spectra were recorded and overall fluctuation amplitude levels measured on the centerline, and in the shear layer, of the laminar boundary layer jet at various axial positions. The spectra, shown in Figures 28 and 29, show that at x/D = 1 the jet is laminar on the centerline and in the shear layer. Fluctuation measurements at x/D = 1 shown in Figures 32 and 33 confirm this.

If the nozzle boundary layer Reynolds number at the

exit of the jet based on momentum thichness (Re_θ) is greater than or equal to the critical Reynolds number ($Re_{\theta\ crit}$), then a small disturbance would cause the boundary layer of the jet to go into transition to turbulence. However, if Re_θ was below $Re_{\theta\ crit}$, then a turbulent boundary layer could only be simulated by introducing some type of near random excitation.

The Reynolds number Re_θ was calculated to be $Re_\theta \approx 110$. Laufer and Vrebalovich (11) have measured the critical Reynolds number of a flat plate boundary layer flow with a freestream Mach number of M = 2.2 (no pressure gradient) to be $Re_{\theta\ crit} \approx 180$. In the presence of a favorable pressure gradient, which exists in the M = 2.1 perfectly expanded nozzle used in this study, $Re_{\theta\ crit}$ could be expected to have a higher value. Since the Reynolds number (Re_θ) of the present experiment is below $Re_{\theta\ crit} \approx 180$, the boundary layer is stable and cannot be tripped. Turbulence in the boundary layer can only be simulated by artificial means. The method used in this study to simulate a turbulent boundary layer, and hence obtain a turbulent shear layer, will be referred to as "exciting" the boundary layer of the laminar boundary layer jet.

To excite the boundary layer, the nozzle wall was coated with grit of average diameter 40 μm, for the first attempt extending from the throat to the exit. With the same hot-wire, spectra and measurements similar to those

above were recorded, the spectra shown in Figures 30 and 31 and the measurements shown in Figures 32 and 33.

The hot-wire spectrum in the shear layer at x/D = 1 (Figure 31) show a fully developed turbulent spectrum, and the fluctuation level (Figure 33) has been increased by a factor of seven over the laminar boundary layer case. However, at x/D = 0.5, the fluctuation level on the centerline of the grit coated nozzle is approximately the same as the centerline fluctuation level of the laminar nozzle at x/D = 1 (Figure 32). This is an indication of flow fluctuation content similar to laminar flow in the core of the jet with the grit excited boundary layer.

B.2. Flow Fluctuation Measurements

Measurements of the coherent fluctuations using the glow exciter on the jet with the grit excited boundary layer were precluded because the flow fluctuations would not phase lock with the exciter. Apparently the excitation level of the glow discharge was significantly below that produced by the grit.

Axial wave evolution measurements, bandpassed at St = 0.20, with no glow excitation were performed. The measurements (Figure 34) were made at a constant radial location of r/D = 0.5, and at the radial location of maximum hot-wire fluctuation voltage, and were normalized with respect to the exit fluctuations.

Troutt and McLaughlin (9) made similar measurements

(Figure 35) on a moderate Reynolds number M = 2.1 jet with a laminar boundary layer, using the same type of hot-wire probe used in this study, at a constant radial location in the middle of the shear layer, but closer to the centerline than r/D = 0.5. McLaughlin et al. (3) performed similar measurements, using a hot-film probe, on a conventional high Reynolds number M = 2.0 jet along the nozzle lip line (r/D = 0.5), the data shown in Figure 35.

Examination of Figure 34 shows that a higher ratio of maximum to exit fluctuations is obtained when the probe is positioned above the lip line. Figures 34 and 35 are qualitatively similar, which suggests that the difference between the two sets of data presented in Figure 35 could be due more to probe positioning (the difference in Reynolds number must also be considered) than to the type of probe used. The ratio of maximum to exit flow fluctuation amplitudes for the excited boundary layer jet (Figure 34) is lower than that obtained with either a laminar boundary layer moderate Reynolds number jet, or a conventional high Reynolds number jet. This difference is probably due to the relatively high level of turbulence introduced into the shear layer by the grit.

To try to reduce the amount of excitation introduced by the grit, the amount of grit was reduced to coat only the nozzle surface extending from the exit to about 10 mm into the nozzle. This had little effect on the hot-wire

spectra, or on the results of the axial wave evolution measurements, so they are not included in this report.

CHAPTER V

CONCLUSIONS AND RECOMMENDATIONS

A. CONCLUSIONS

From the measurements made on the laminar boundary layer jet, the following conclusions can be drawn:

1. The dual electrode glow exciter operating in or out of phase causes the n = 0 or n = $\pm$1 modes to be predominant. Separation of modes using this technique is very good.
2. Using this mode separation technique, hitherto impossible direct comparisons of the wave evolution and noise radiation characteristics of the n = 0 and n = $\pm$1 modes can now be made.
3. Artificial excitation has a significant effect on the mean flow when compared to a natural jet. The effect on the mean flow of in phase or out of phase excitation is very similar, however, in phase excitation causes slightly higher thickening of the shear layer.
4. The higher amplitude level of the flow fluctuations in the shear layer caused by the n = $\pm$1 mode is an indication that it is the preferred mode of the jet. The coherence of the n = $\pm$1

mode instability after the amplitude peak contrasted with the low coherence of the n = 0 mode shear layer disturbance also indicates that the n = $\pm$1 mode is preferred, since it is capable of convecting much longer distances downstream. However, the greater overall and coherent noise levels of the n = 0 mode demonstrate that at the M = 2.1, Re = 68,000 condition the n = 0 mode of instability is significantly more effective in producing noise radiation.

From the experiments performed on the jet with the grit excited boundary layer, the following deductions seem appropriate:

1. The amount and size of grit used in this study was enough to introduce a high level of turbulence into the shear layer of the flow but the core of the jet remained approximately laminar on exit.
2. Enough turbulence was introduced into the shear layer so that the glow discharge technique was not feasible. By the time the flow reached the nozzle exit, there was a broad spectrum of relatively high amplitude fluctuations present due to the grit excitation, and the disturbance excited by the glow could not be distinguished from the other disturbances.
3. The qualitative similarity of the data obtained by the hot-wire and hot-film probes is encouraging. However, further experimentation is needed

before the hot-film probe can be considered to be as quantitatively reliable in supersonic flows as the hot-wire.

B. Recommendations

To assist in understanding the role that the n = 0 and n = $\pm$1 modes have in the noise generation process, the author recommends that further SPL directivity measurements be performed on this same jet, varying only the Reynolds number, and exciting the flow with the dual glow in or out of phase. Sound pressure level contour data, obtained under the same conditions, would also be helpful in trying to understand the effect on noise generation by the various modes.

In future attempts to excite the boundary layer, the author recommends that much smaller size grit be used, so that a very small amplitude disturbance is introduced into the shear layer. This would probably allow the acquisition of coherent wave evolution data. The effect on the mean flow of the jet by the grit should be determined. An approximately linear shear layer growth rate would indicate that the shear layer of the excited boundary layer jet develops similarly to the shear layer in a conventional high Reynolds number flow.

REFERENCES CITED

(1) Morris, P.J. and Tam, C.K.W. "Near and Far Field Noise from Large-Scale Instabilities of Axisymmetric Jets,: A.I.A.A. Paper No. 77-1351, 1977.

(2) Morrison, G.L. "Flow Instability and Acoustic Radiation Measurements of Low Reynolds Number Supersonic Jets," Ph.D. Dissertation, Oklahoma State University, Stillwater, Oklahoma, 1977.

(3) McLaughlin, D.K., Seiner, J.M. and Liu, C.H., "On the Noise Generated by Large Scale Instabilities in Supersonic Jets," A.I.A.A. Paper No. 80-0964, 1980.

(4) Troutt, T.R. "Measurements of the Flow and Acoustic Properties of a Moderate Reynolds Number Supersonic Jet," Ph.D. Dissertation, Oklahoma State University, Stillwater, Oklahoma, 1978.

(5) Tester, B.J., Morris, P.J., Lau, J.C. and Tanna, H.K. "The Generation, Radiation and Prediction of Supersonic Jet Noise - Volume 1," Technical Report AFAPL-TR-78-85, 1978.

(6) Kovasznay, L.S.G. "The Hot-Wire Anemometer in Supersonic Flow," J. Aero. Sci., Vol 17, No. 9 (September, 1950), pp. 565-572.

(7) McLaughlin, D.K., Morrison, G.L., and Troutt, T.R., "Reynolds Number Dependence in Supersonic Jet Noise," AIAA J., Vol. 15 (1977), pp. 526-532.

(8) Morrison, G.L. and McLaughlin, D.K., "Instability Processes in Low Reynolds Number Supersonic Jets," A.I.A.A. Paper No. 80-4064, 1980.

(9) Troutt, T.R. and McLaughlin, D.K., "Experiments on the Flow and Acoustic Properties of a Moderate Reynolds Number Supersonic Jet," JFM, 1980.

(10) Hu, T.F., "Flow and Acoustic Properties of Low Reynolds Number Underexpanded Supersonic Jets," Ph.D. Dissertation, Oklahoma State University, Stillwater, Oklahoma, 1981.

(11) Laufer, J. and Vrebalovich, T. "Stability and Transition of a Supersonic Laminar Boundary Layer on an Insulated Flat Plate," J. Fluid Mech., 9,257-99, 1960.

APPENDIX A

FIGURES

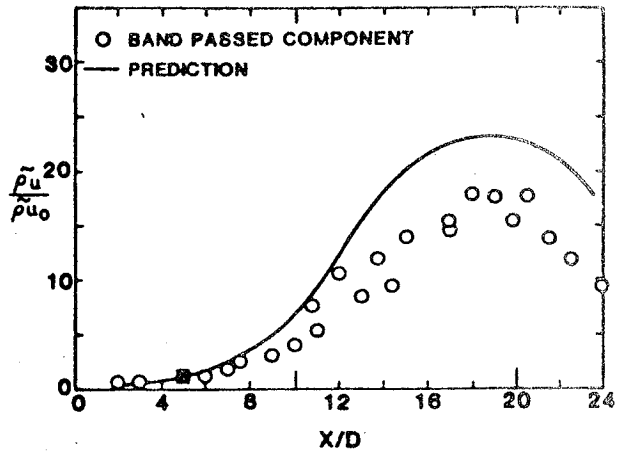

Figure 1. Axial Distribution of Mass-Velocity Fluctuation Amplitude in the Jet Shear Layer for the M=2.5, Re=8700 Jet, From McLaughlin et al. (3)

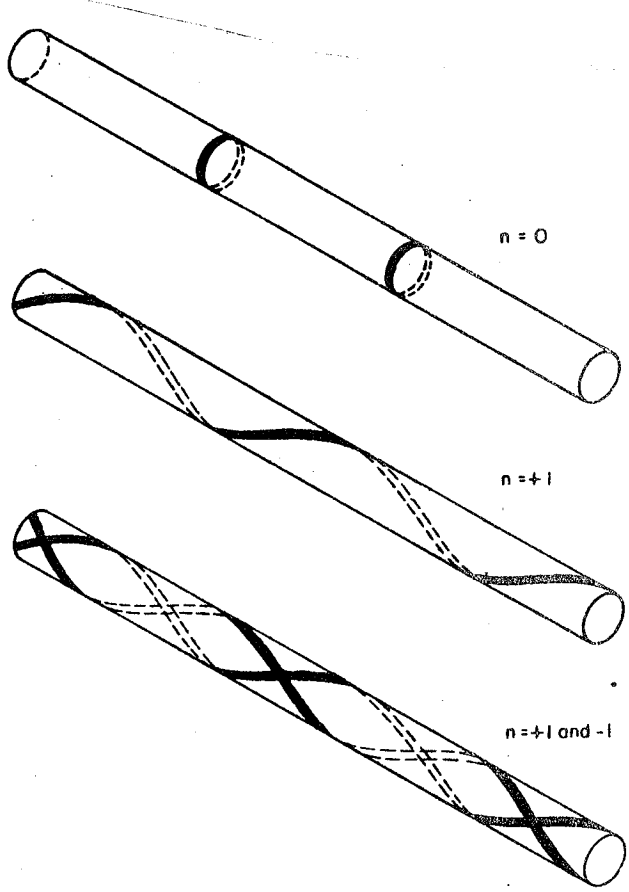

Figure 2. Sketches of Wavefronts of Various Instability Modes

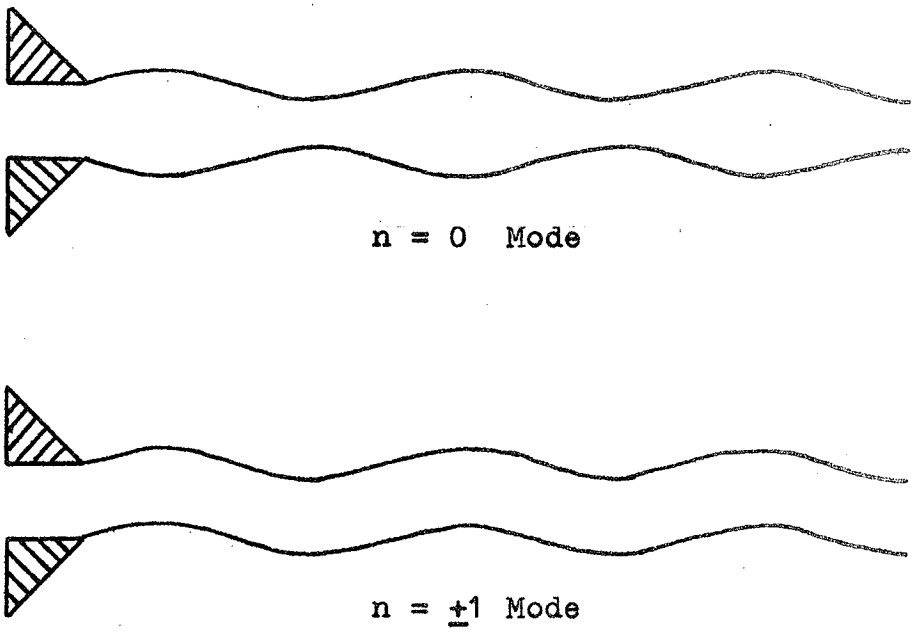

Figure 3. Sketches of Instantaneous Streamline Patterns of Various Instability Modes

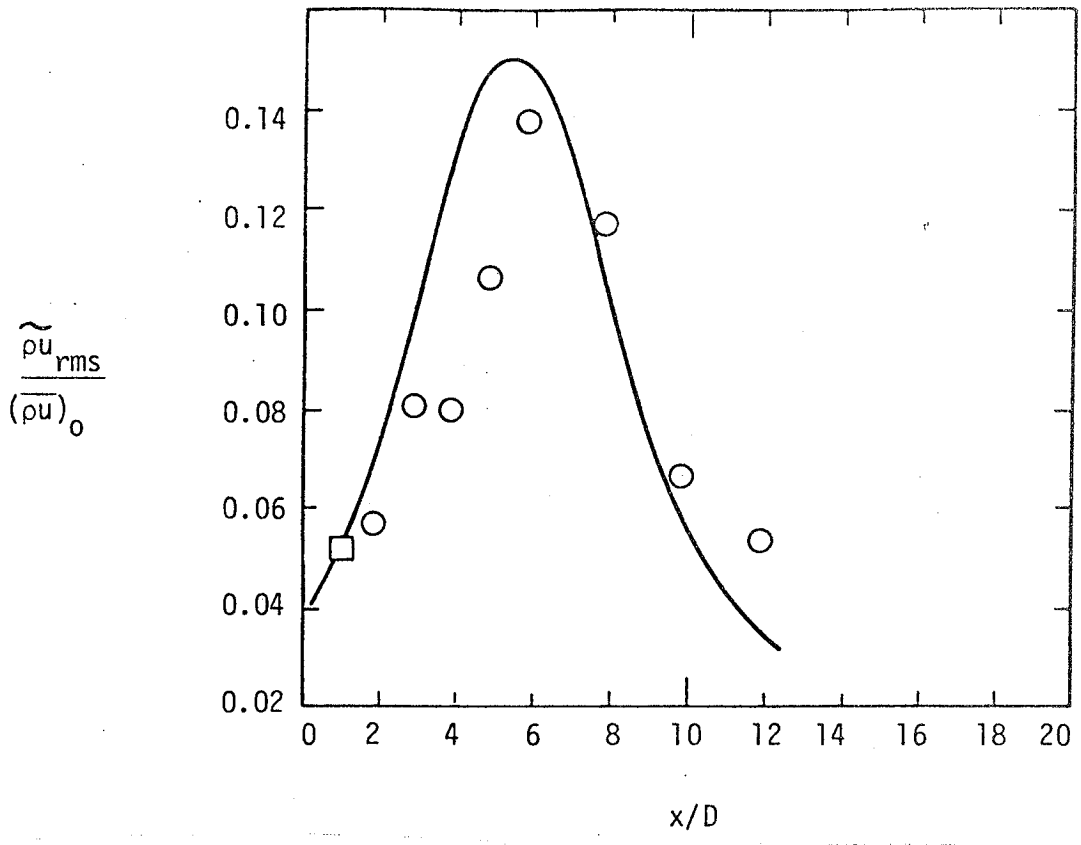

Figure 4. Coherent Mass-Velocity Fluctuation Amplitude in the Jet Shear Layer, St=0.20, Single Glow, Laminar Boundary Layer, From Troutt et al. (9)

○ - Experiment

(—) - Prediction

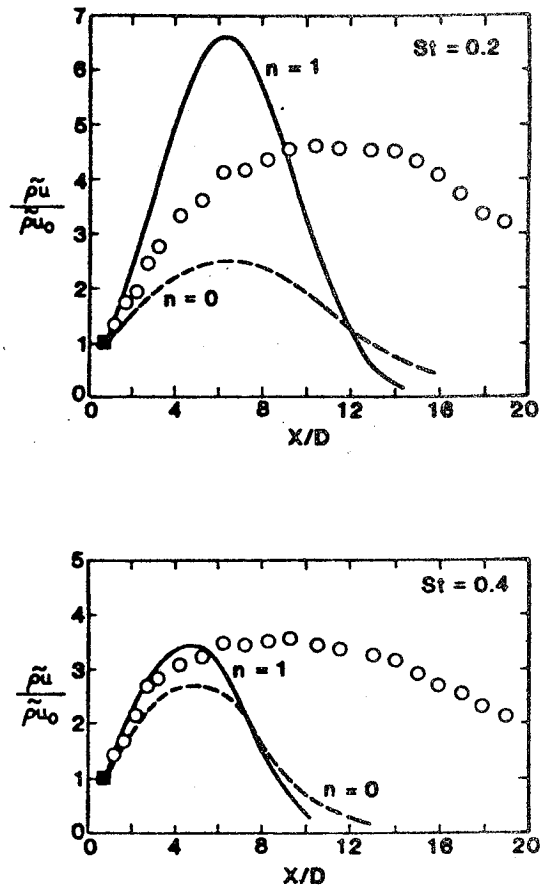

Figure 5. Axial Distribution of Mass Velocity Fluctuation Amplitude in the Jet Shear Layer for an M=2.0, Re=5.2 x 10^6 Jet, From McLaughlin et al. (3)

o - Experiment

(—) - Prediction

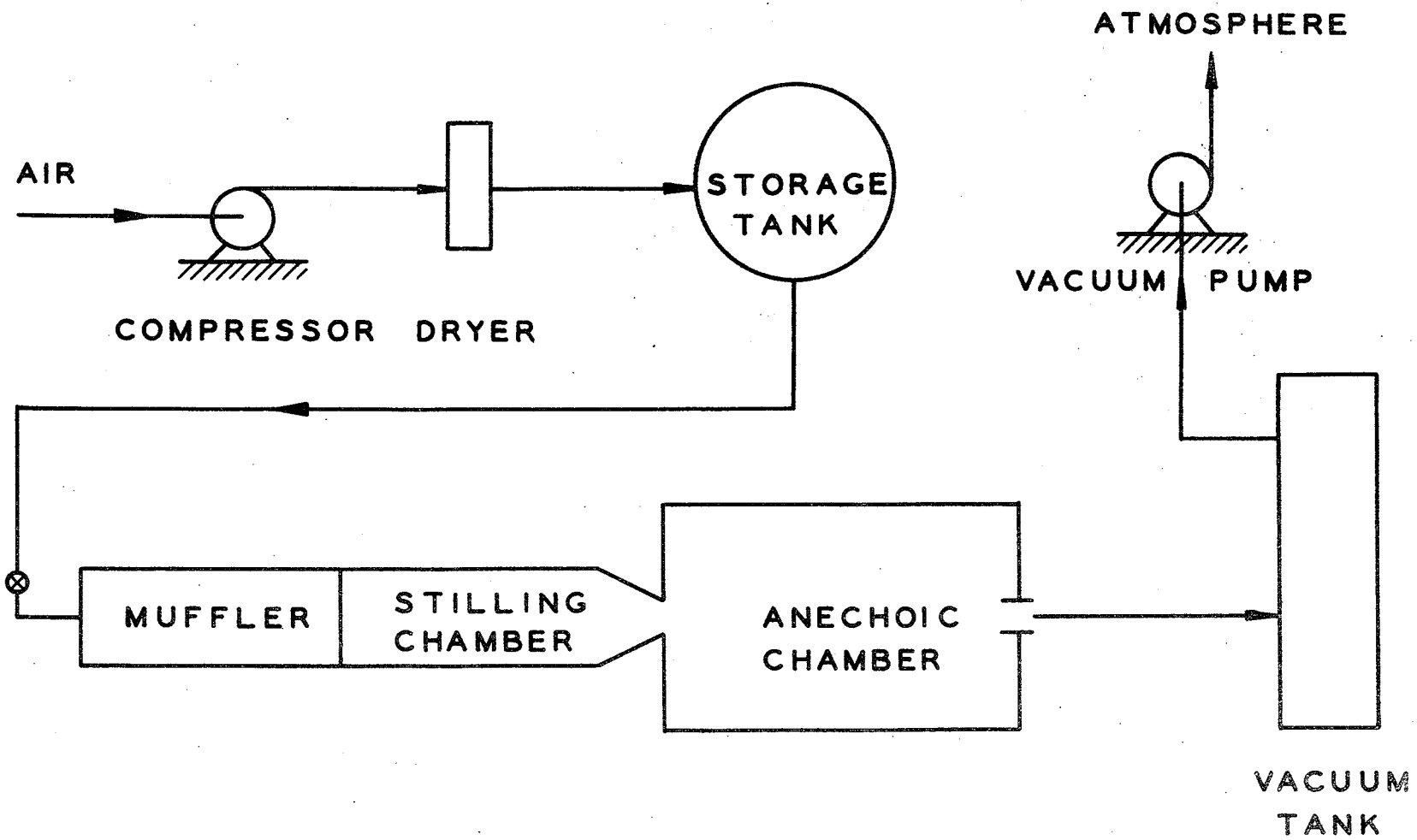

Figure 6. Schematic of Test Facility

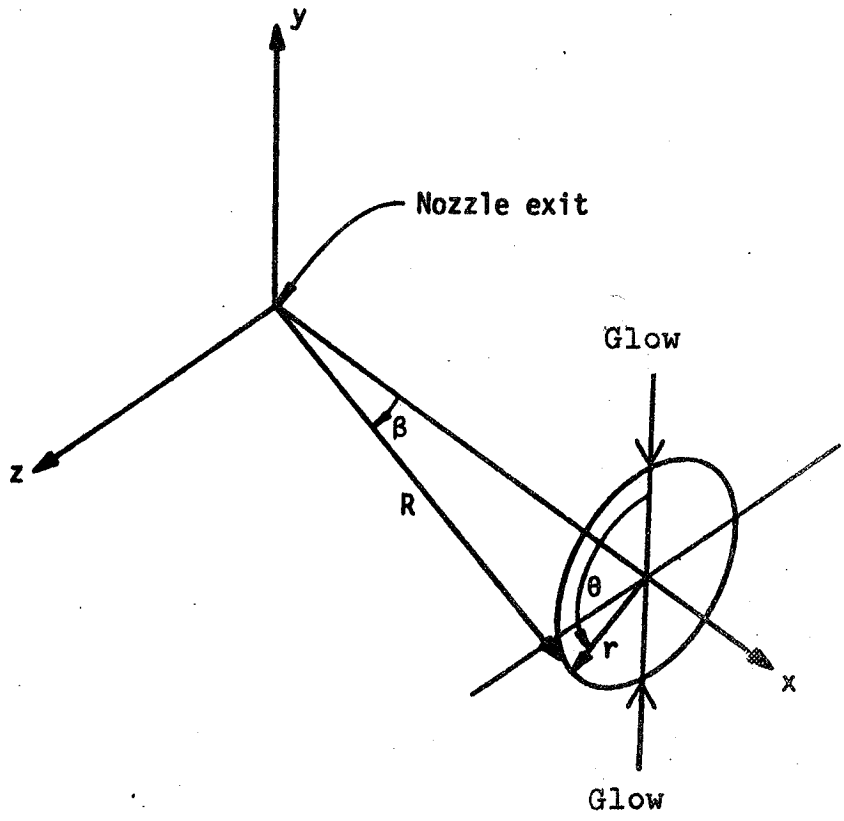

Figure 7. Coordinate System and Glow Orientation

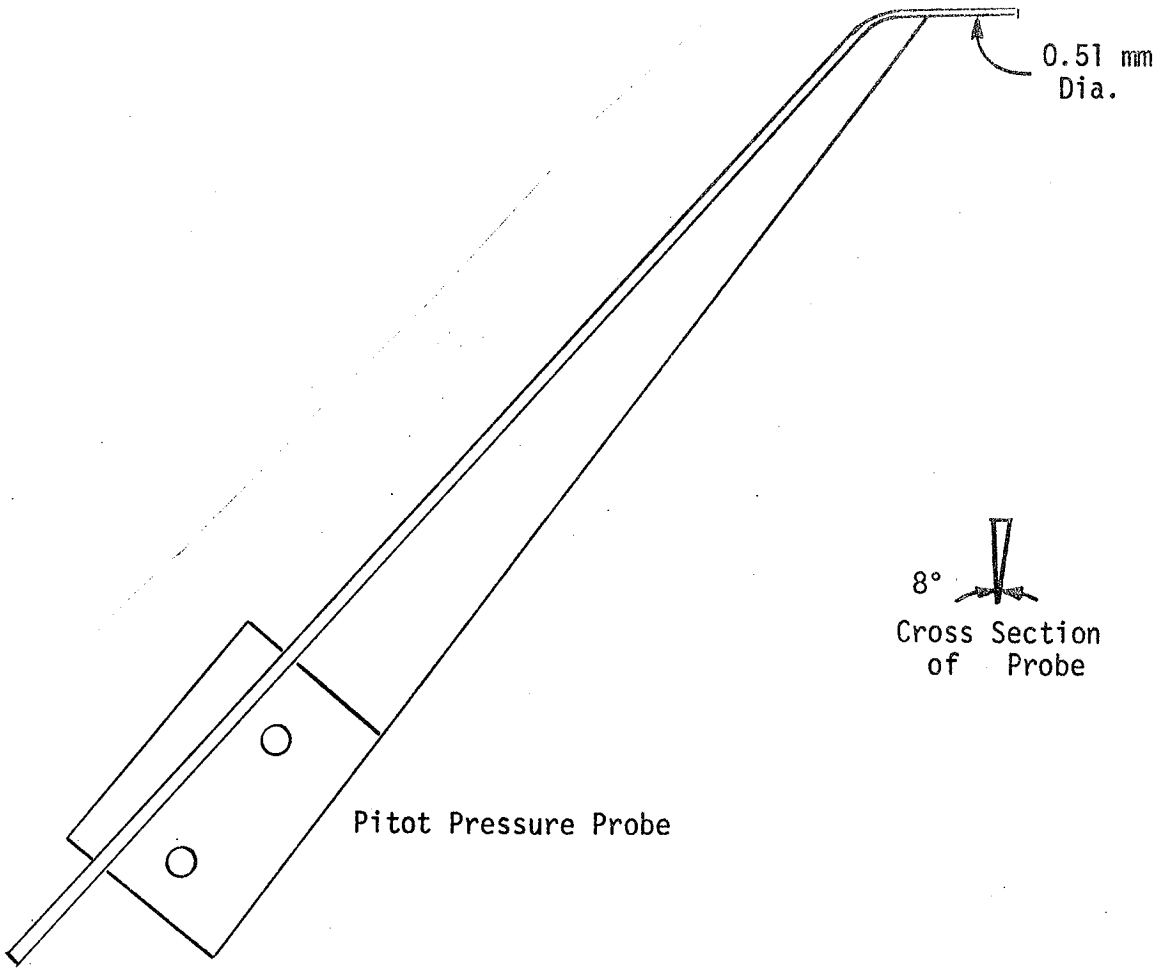

Figure 8. Pitot Pressure Probe, Drawn Full Scale

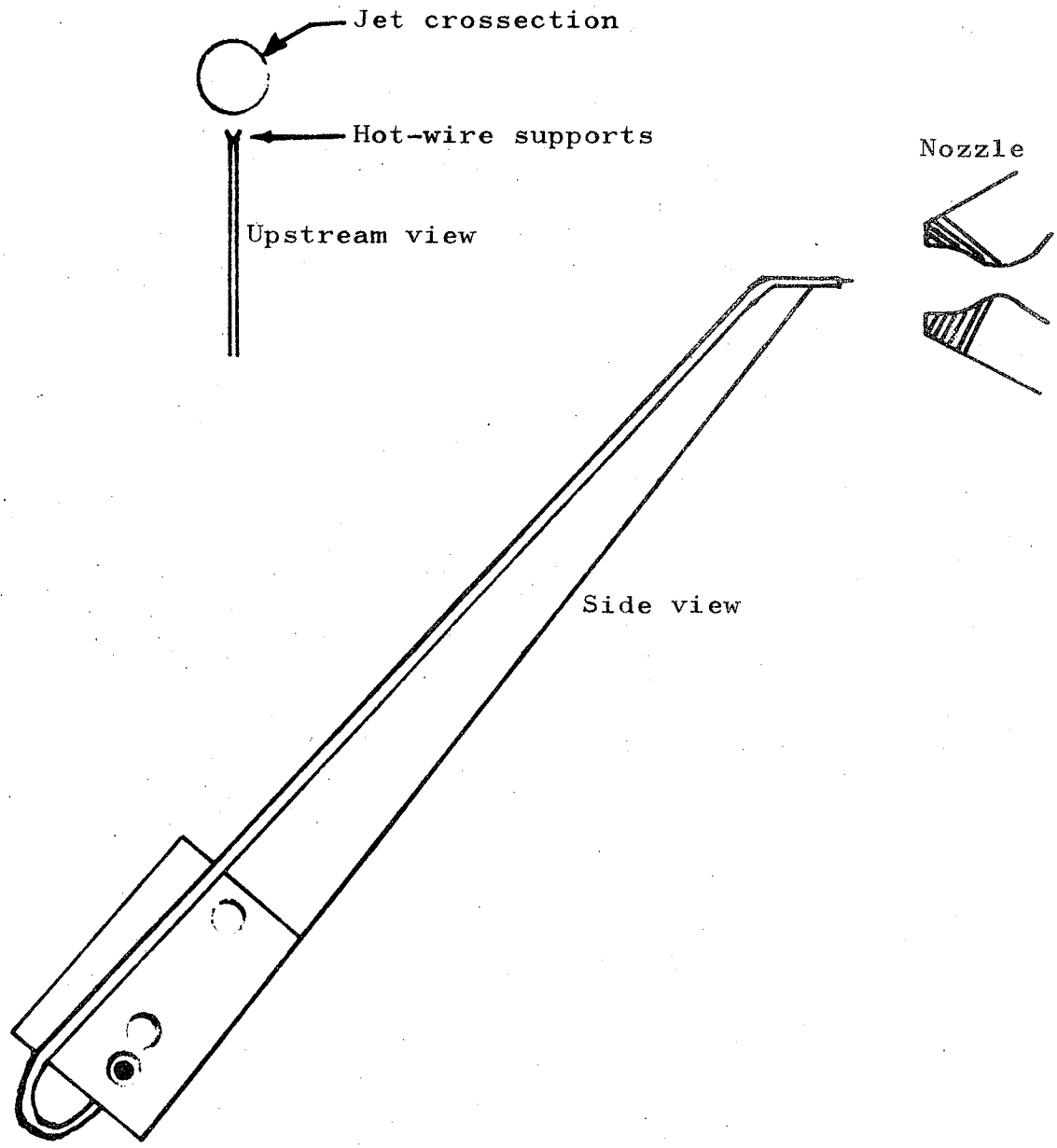

Figure 9. Hot-wire Probe, Full Scale

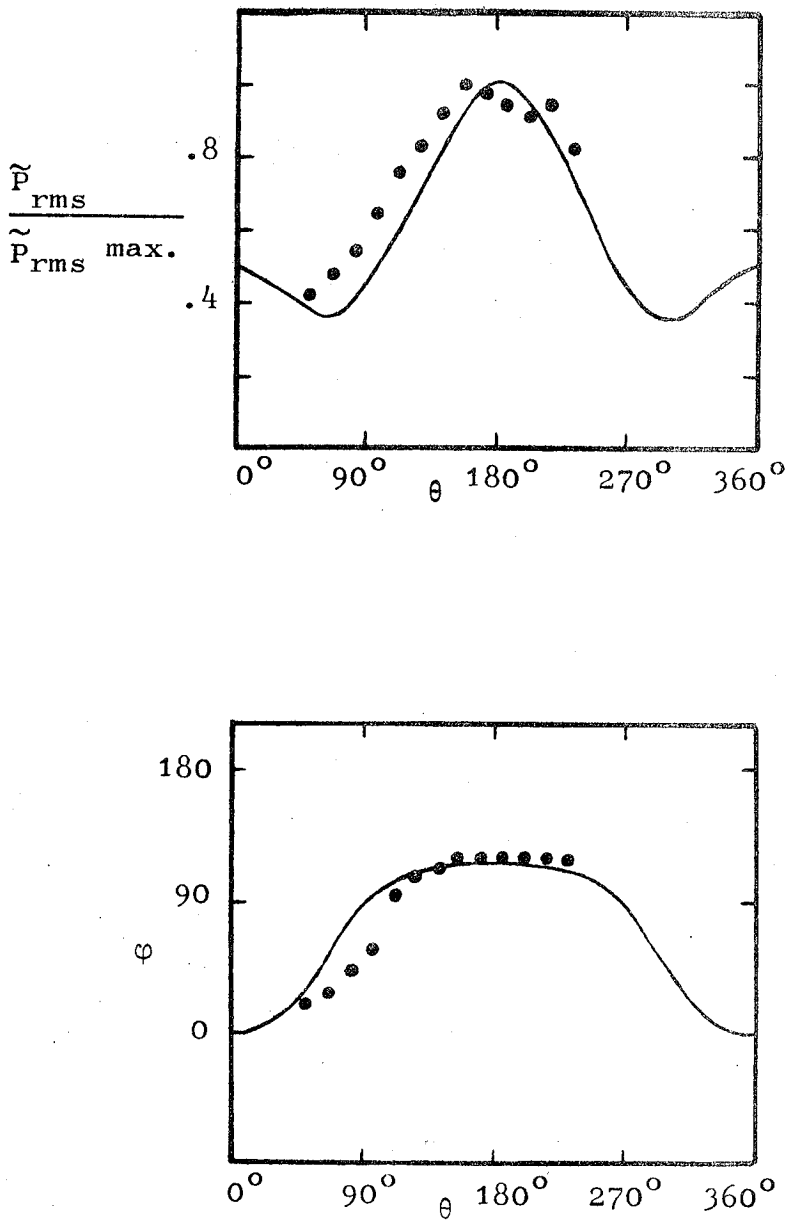

Figure 10. Coherent Sound Pressure Amplitude and Phase Angle as a Function of Azimuthal Angle, St=0.20, Single Glow, From Troutt (4)

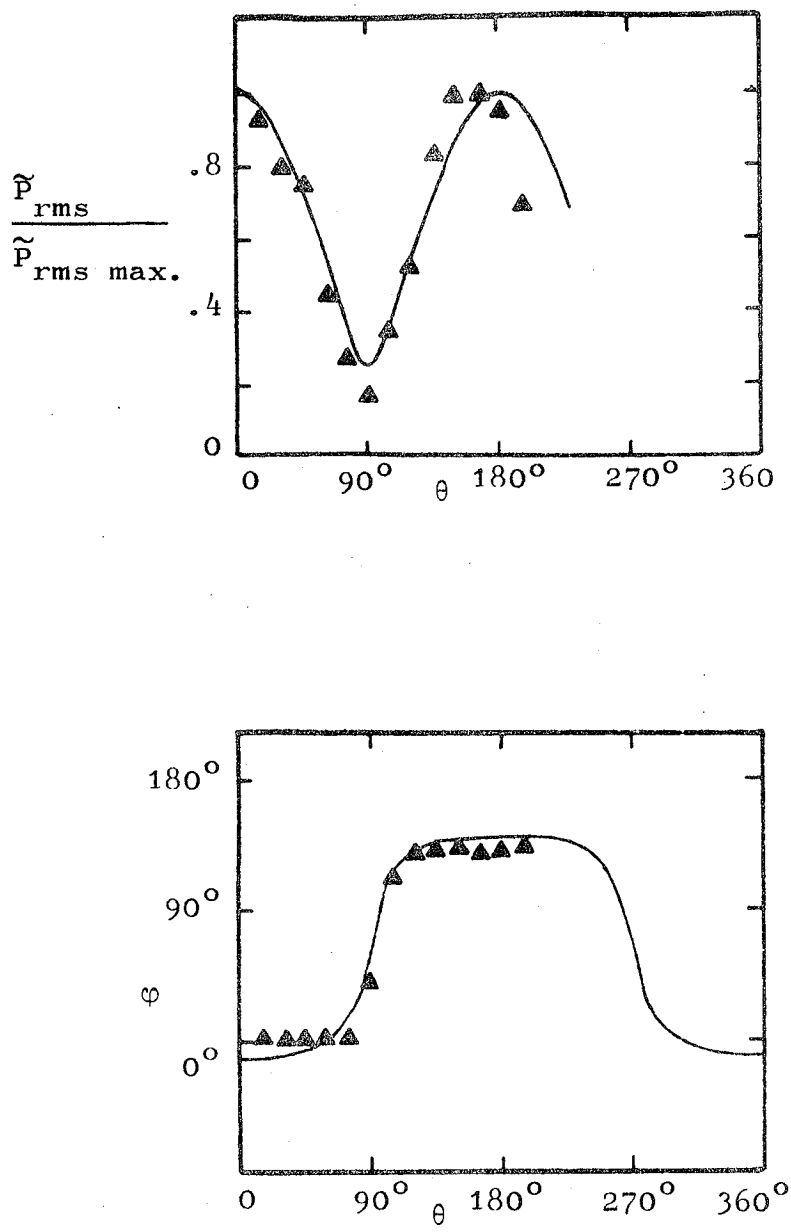

Figure 11. Coherent Sound Pressure Amplitude and Phase Angle as a Function of Azimuthal Angle, St=0.38, Single Glow, From Troutt (4)

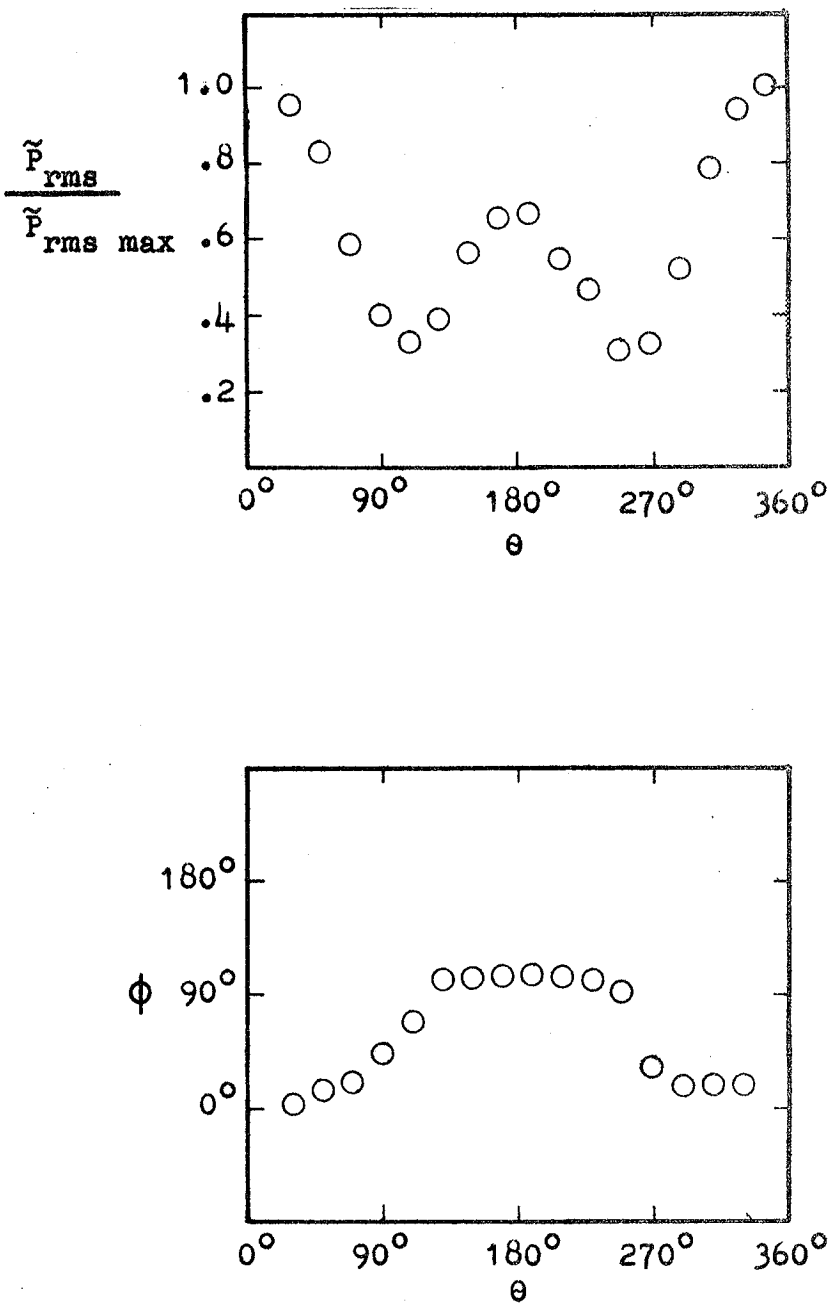

Figure 12. Coherent Sound Pressure Amplitude and Phase Angle as a Function of Azimuthal Angle St=0.38, Single Glow

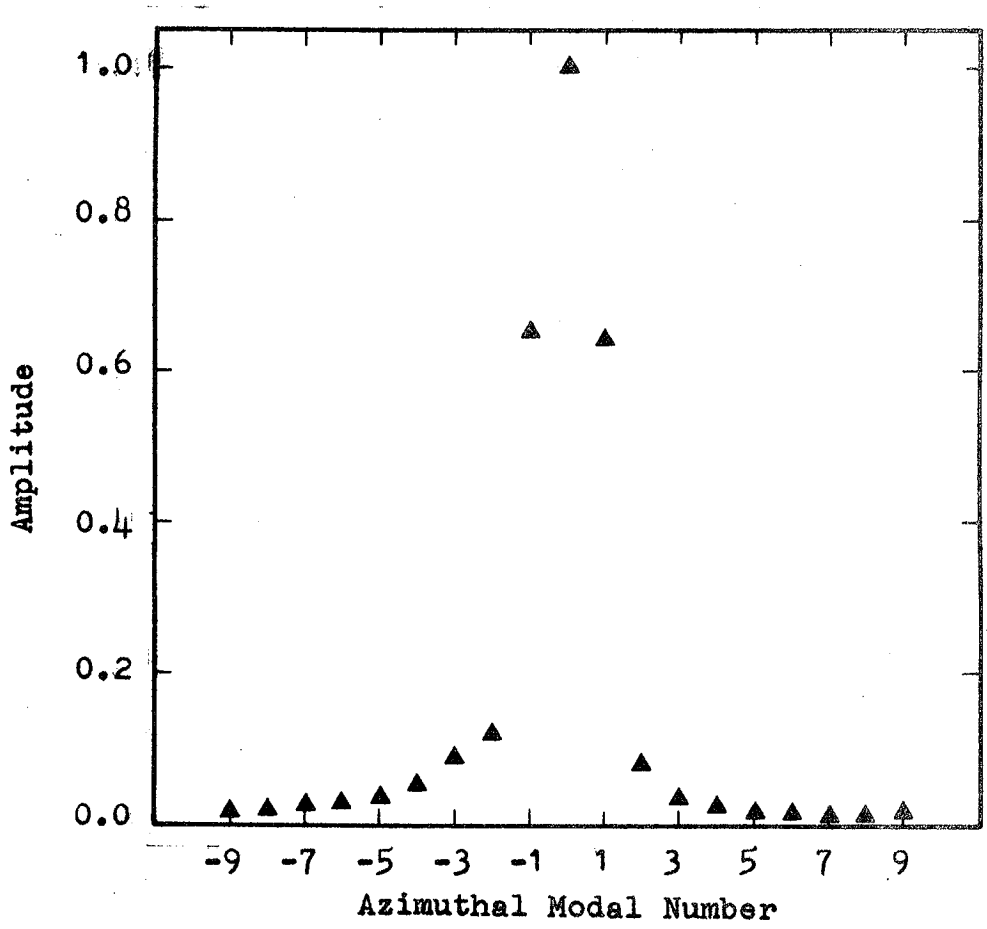

Figure 13. Modal Spectrum of St=0.38, Single Glow Data Shown in Figure 12

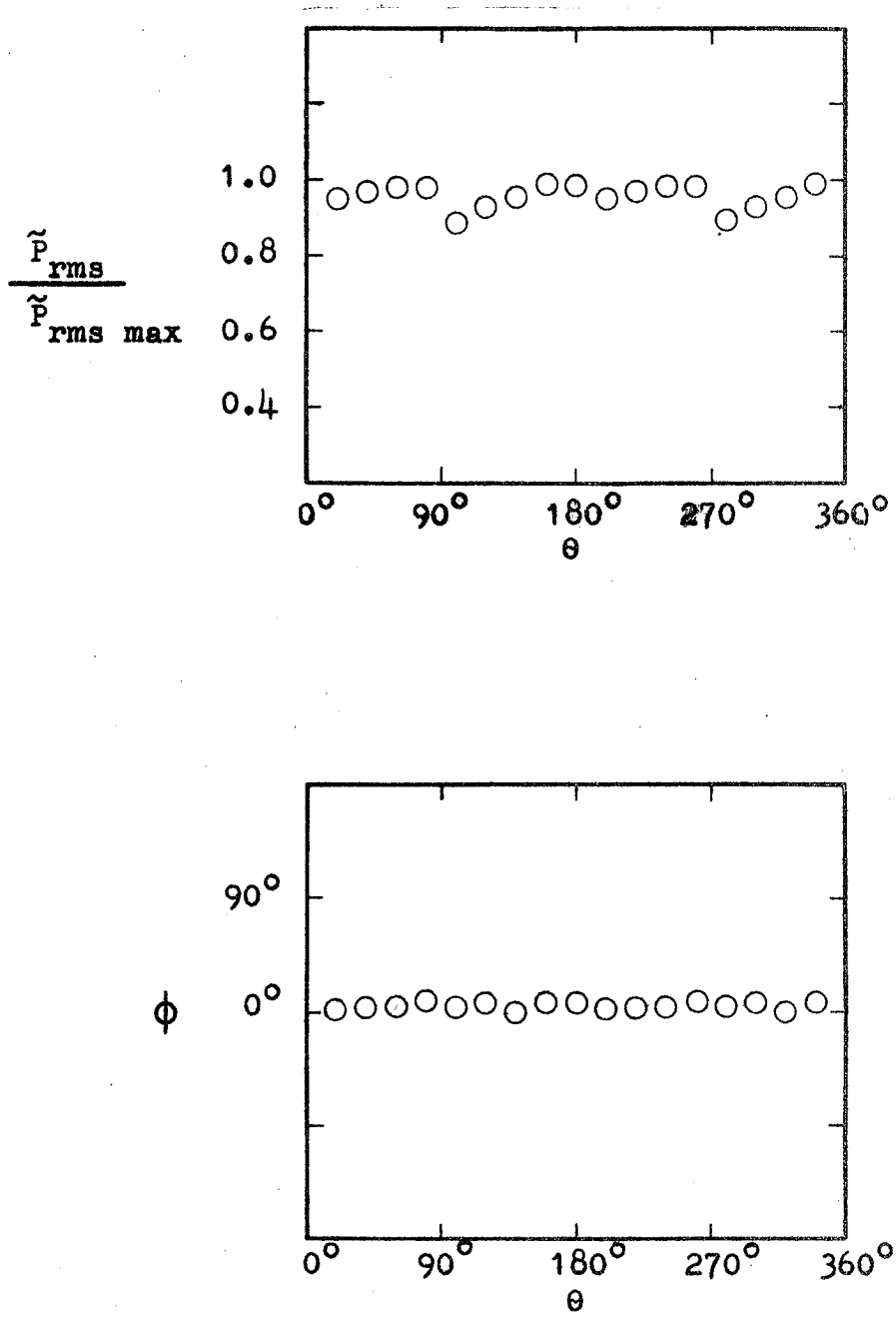

Figure 14. Coherent Sound Pressure Amplitude and Phase Angle as a Function of Azimuthal Angle, St=0.20, Double Glow In Phase

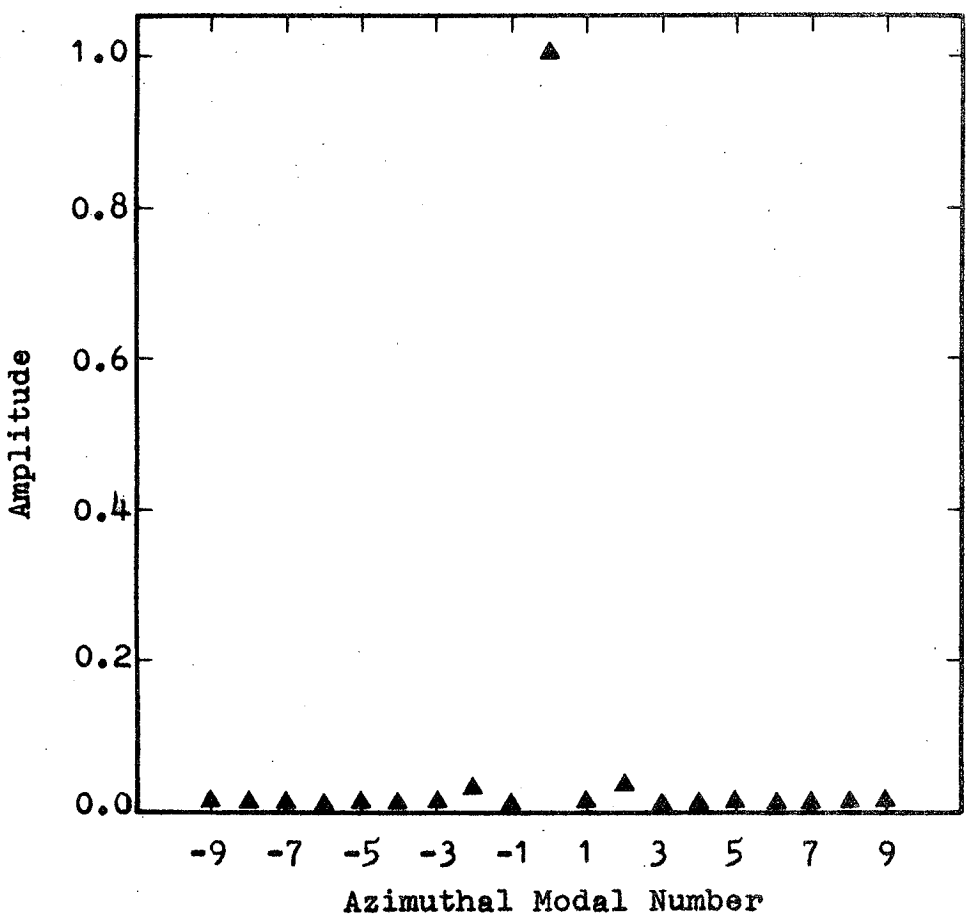

Figure 15. Modal Spectrum of St=0.20, Double Glow In Phase Data Shown in Figure 14

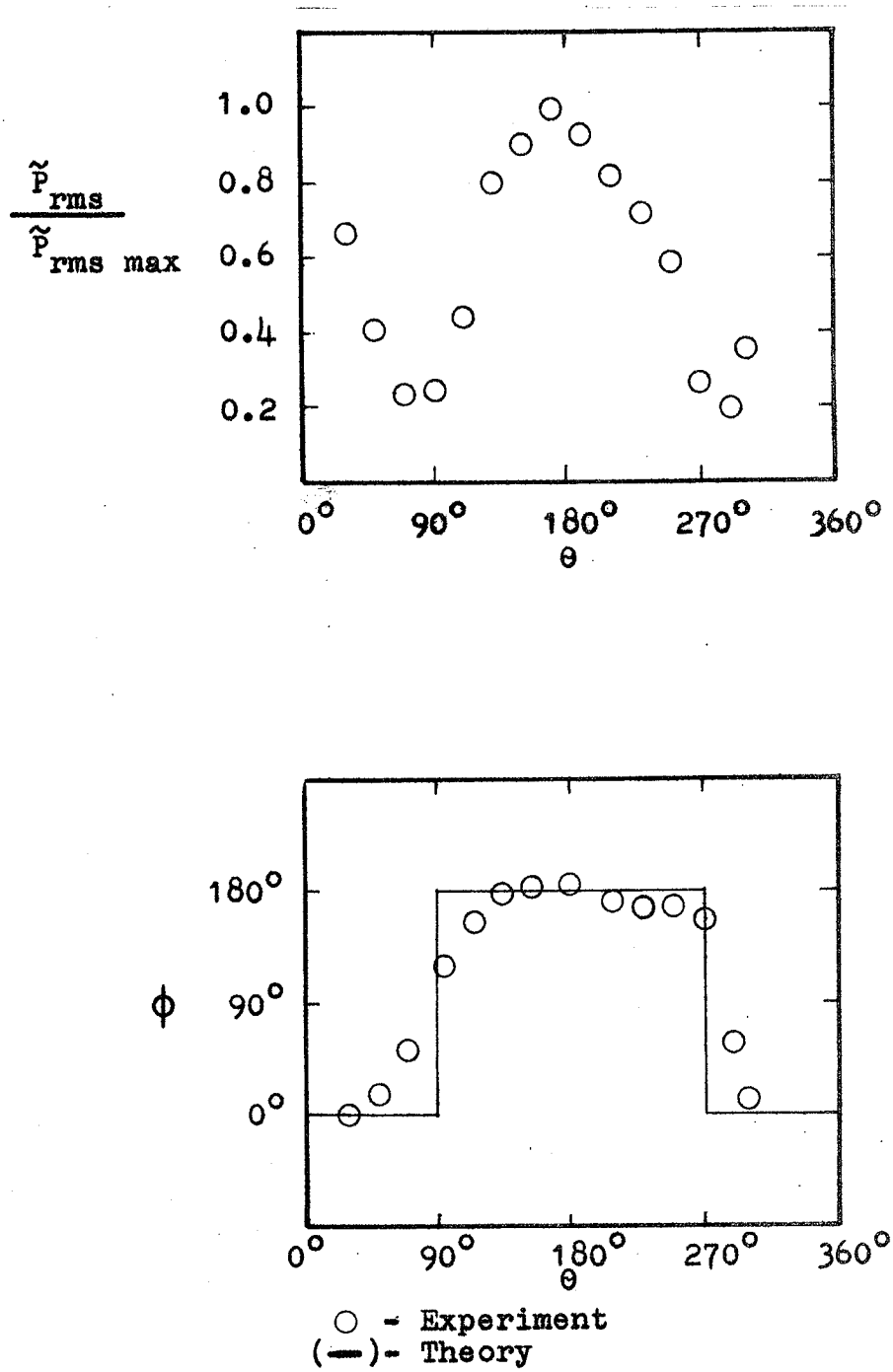

Figure 16. Coherent Sound Pressure Amplitude and Phase Angle as a Function of Azimuthal Angle, St=0.20, Double Glow Out of Phase

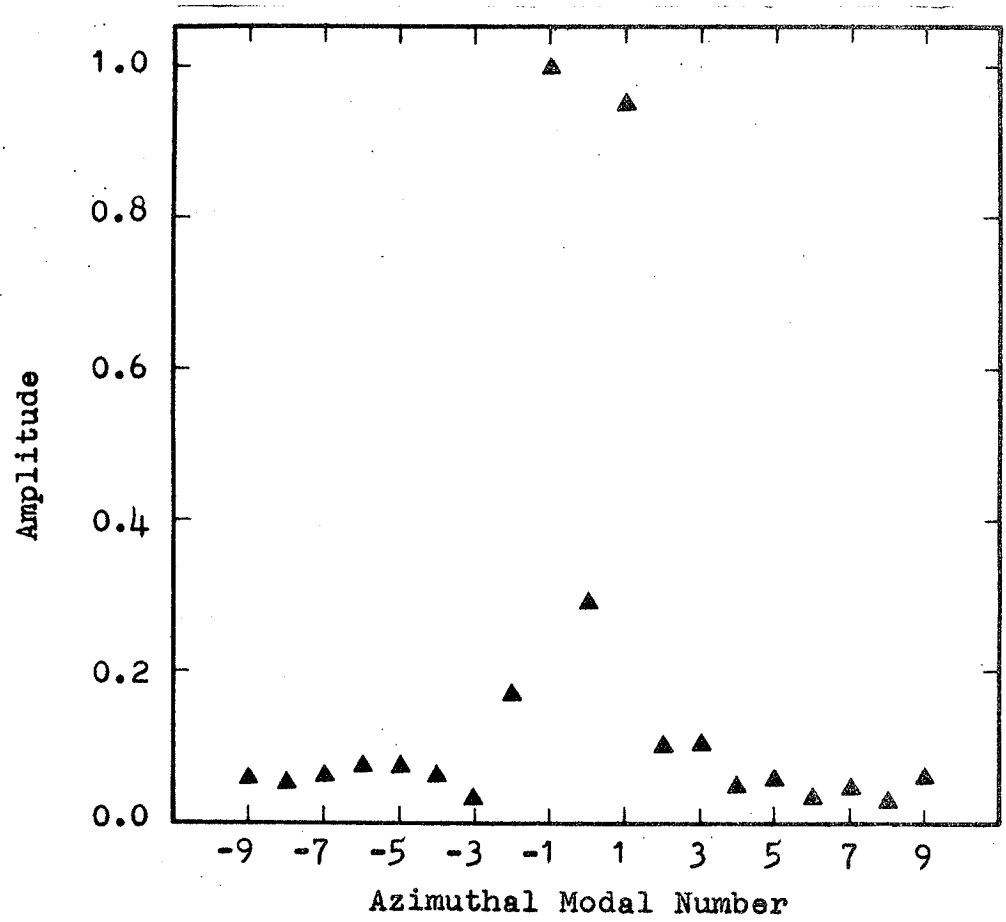

Figure 17. Modal Spectrum of St=0.20, Double Glow Out of Phase Data Shown in Figure 16

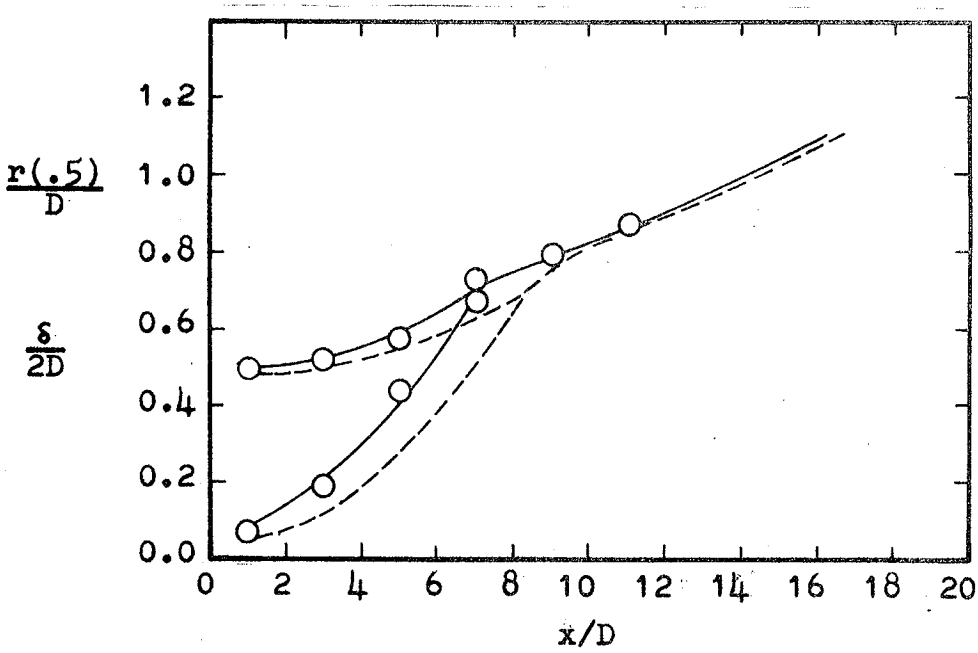

Figure 18. Axial Distribution of Mean Velocity Parameters, St=0.20, Double Glow In Phase, Laminar Boundary Layer

○—○ Excited Jet

---- Natural Jet , From Troutt et al. (9)

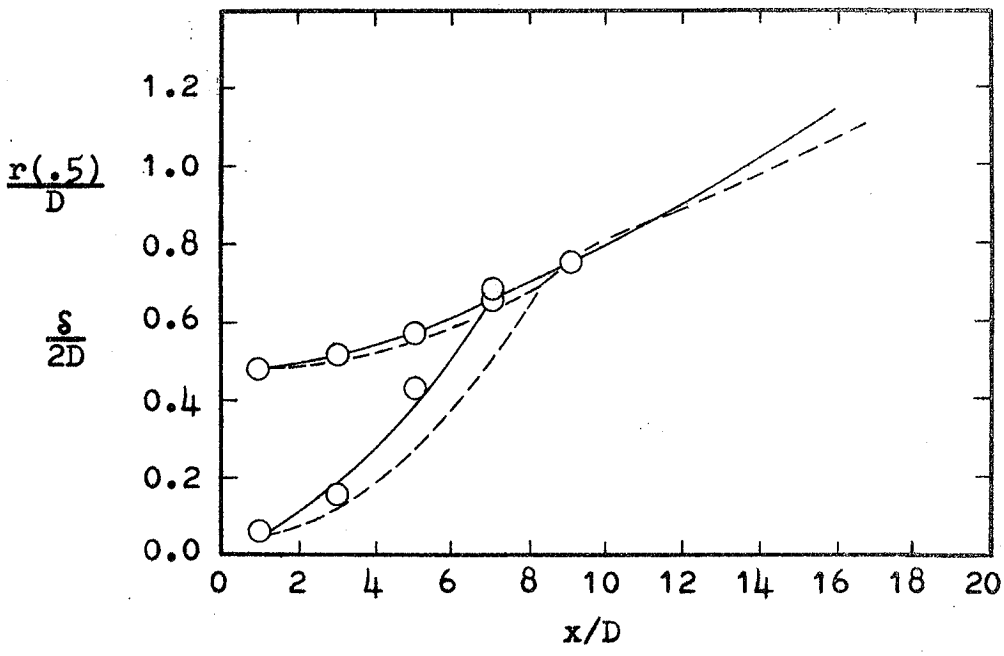

Figure 19. Axial Distribution of Mean Velocity Parameters, St=0.20, Double Glow Out of Phase, Laminar Boundary Layer

○—○ Excited Jet

---- Natural Jet, From Troutt et al. (9)

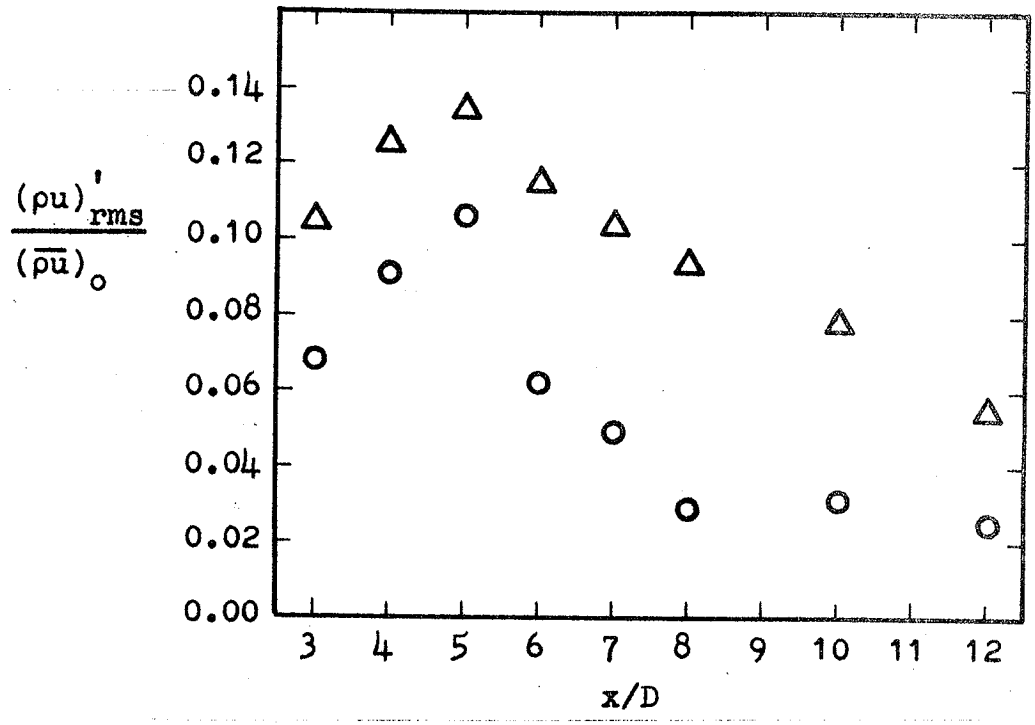

Figure 20. Mass-Velocity Fluctuation Amplitude in the Jet Shear Layer, St=0.23, Double Glow In Phase, Laminar Boundary Layer

O - Coherent Portion

Δ - Overall

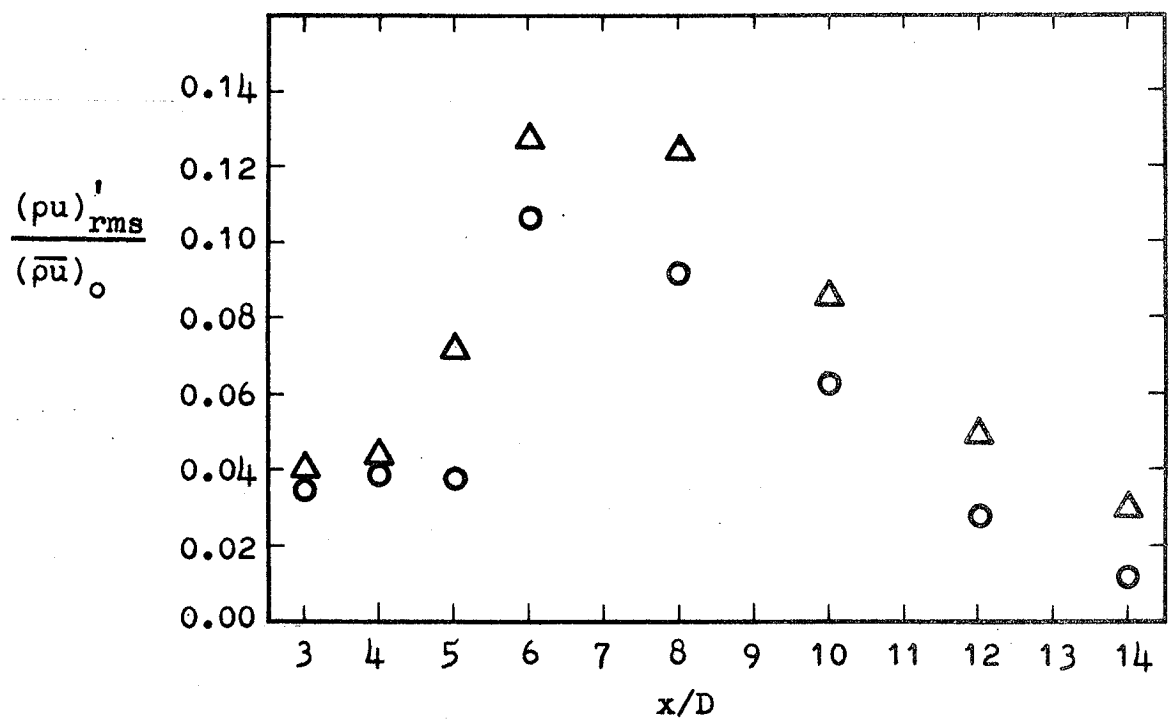

Figure 21. Mass-Velocity Fluctuation on the Jet Centerline, St=0.22, Double Glow In Phase, Laminar Boundary Layer

o - Coherent Portion

Δ - Overall

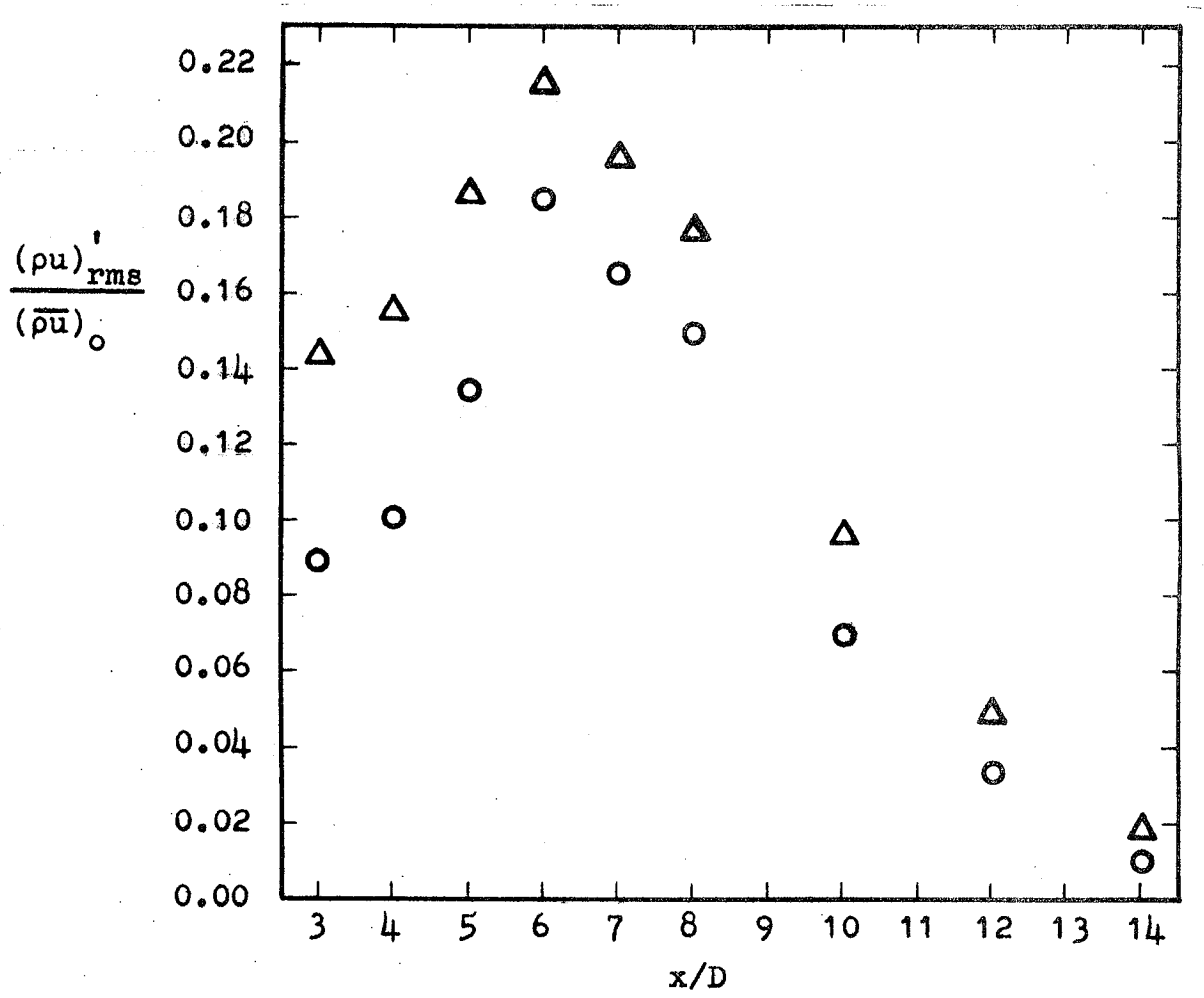

Figure 22. Mass-Velocity Fluctuation Amplitude in the Jet Shear Layer, St=0.22, Double Glow Out of Phase, Laminar Boundary Layer

○ - Coherent Portion

△ - Overall

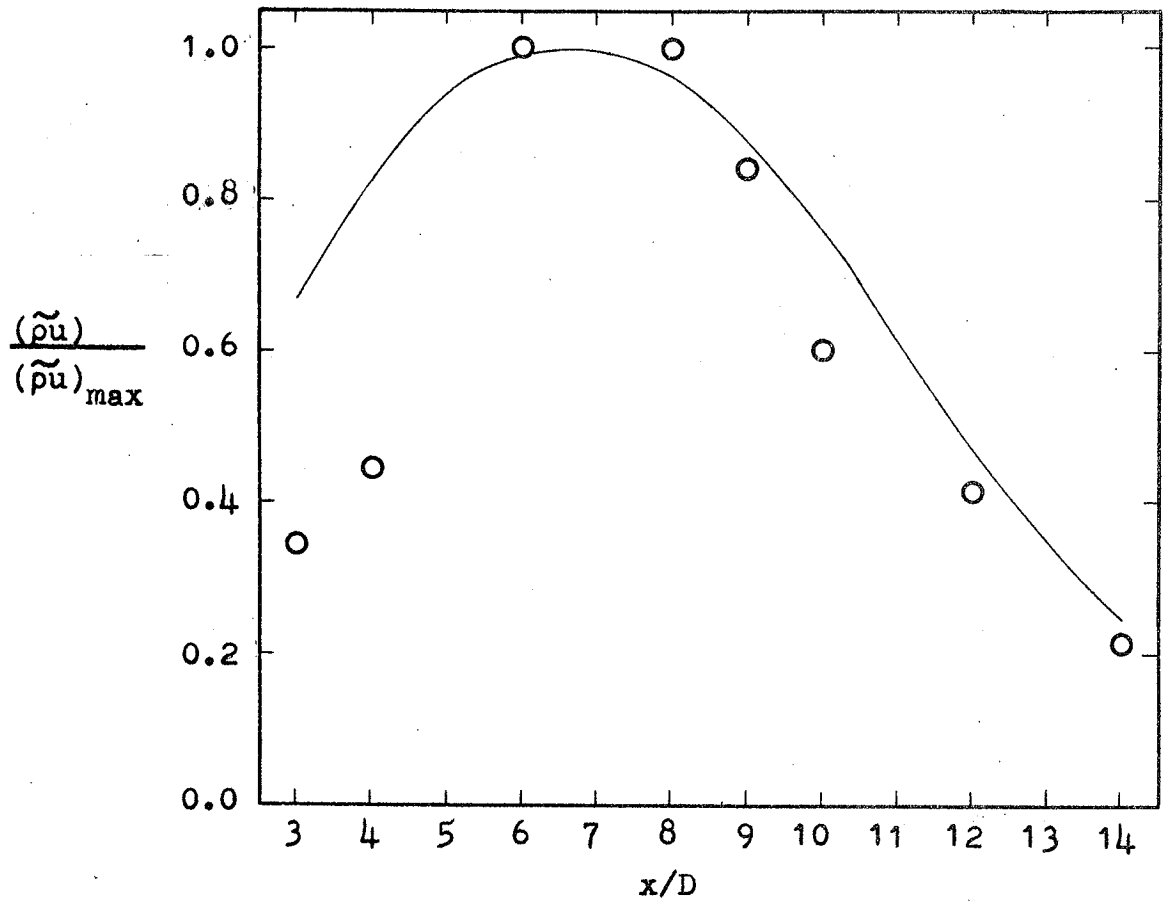

Figure 23. Coherent Mass-Velocity Fluctuation Amplitude on the Jet Centerline, St=0.22, Double Glow In Phase, Laminar Boundary Layer

O - Present Experiment

(—) - Tester et al. Prediction (5)

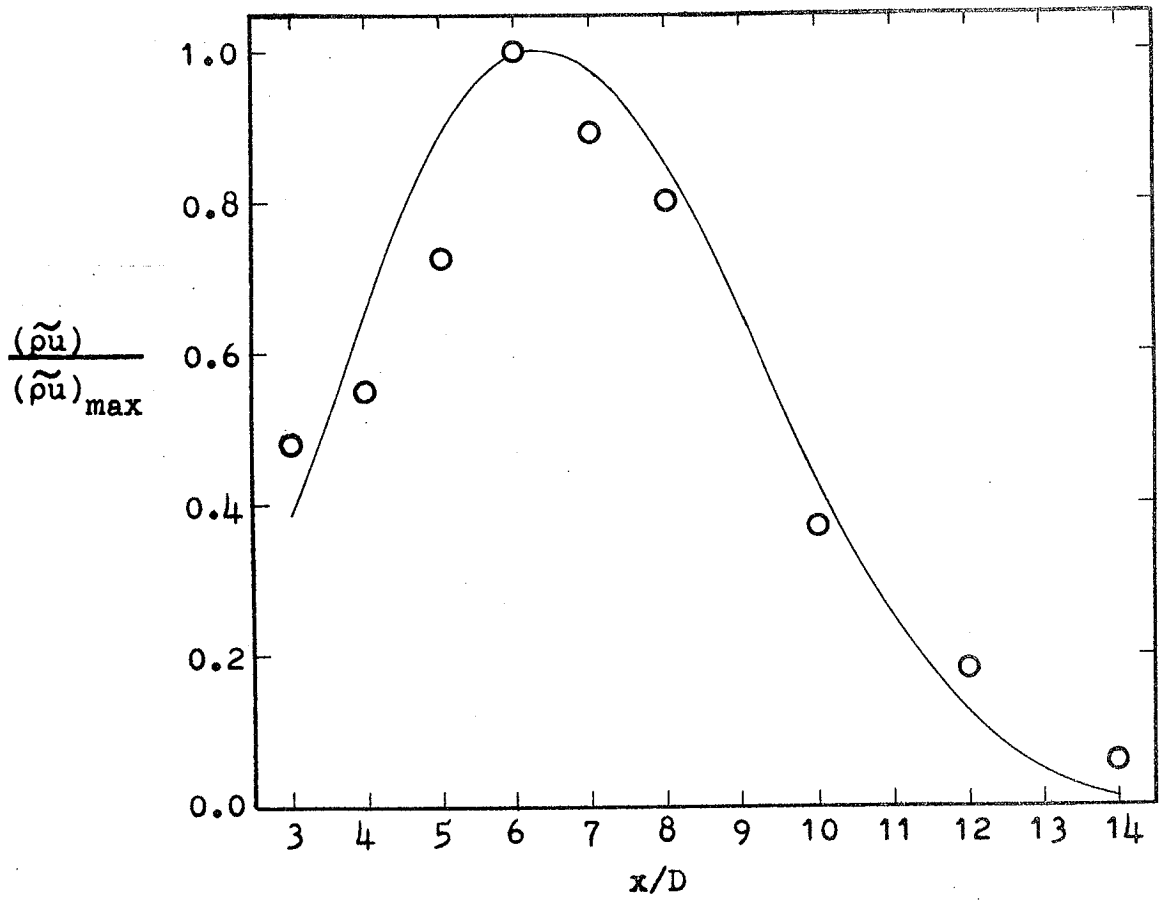

Figure 24. Coherent Mass-Velocity Fluctuation Amplitude in the Jet Shear Layer, St=0.22, Double Glow Out of Phase, Laminar Boundary Layer

O - Present Experiment

(—) - Tester et al. Prediction (5)

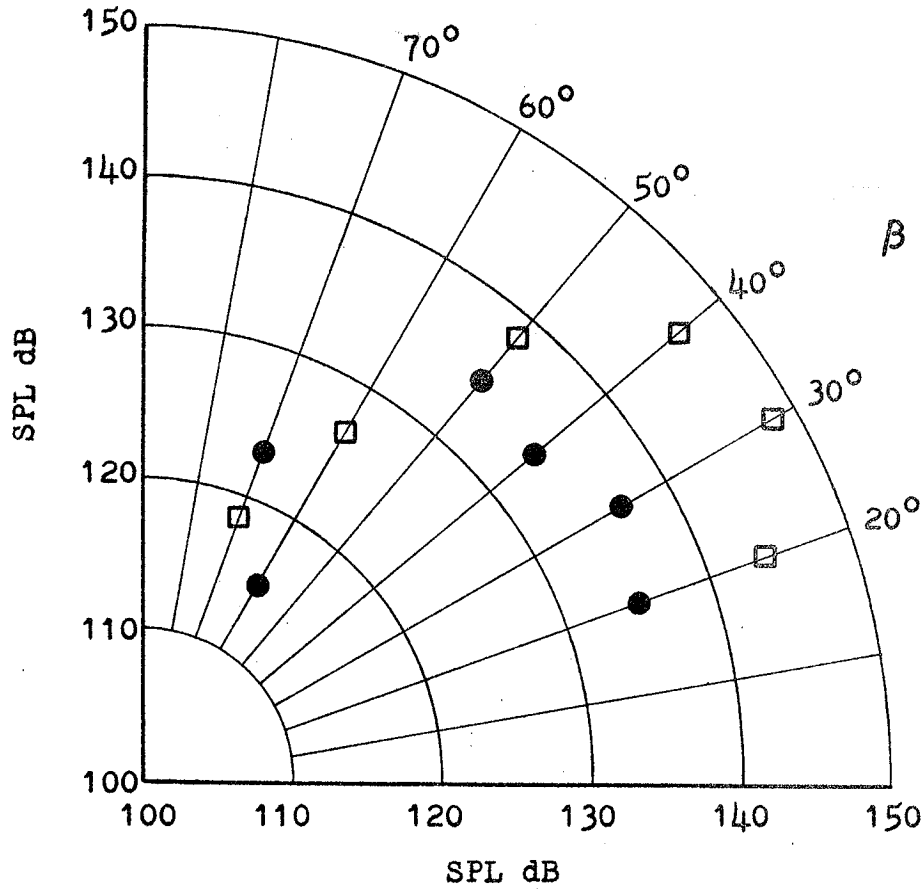

Figure 25. St=0.22 Coherent Sound Pressure Level Directivity Distribution, M=2.1 Perfectly Expanded Jet, R/D=30

□ - Glows In Phase

● - Glows Out Of Phase

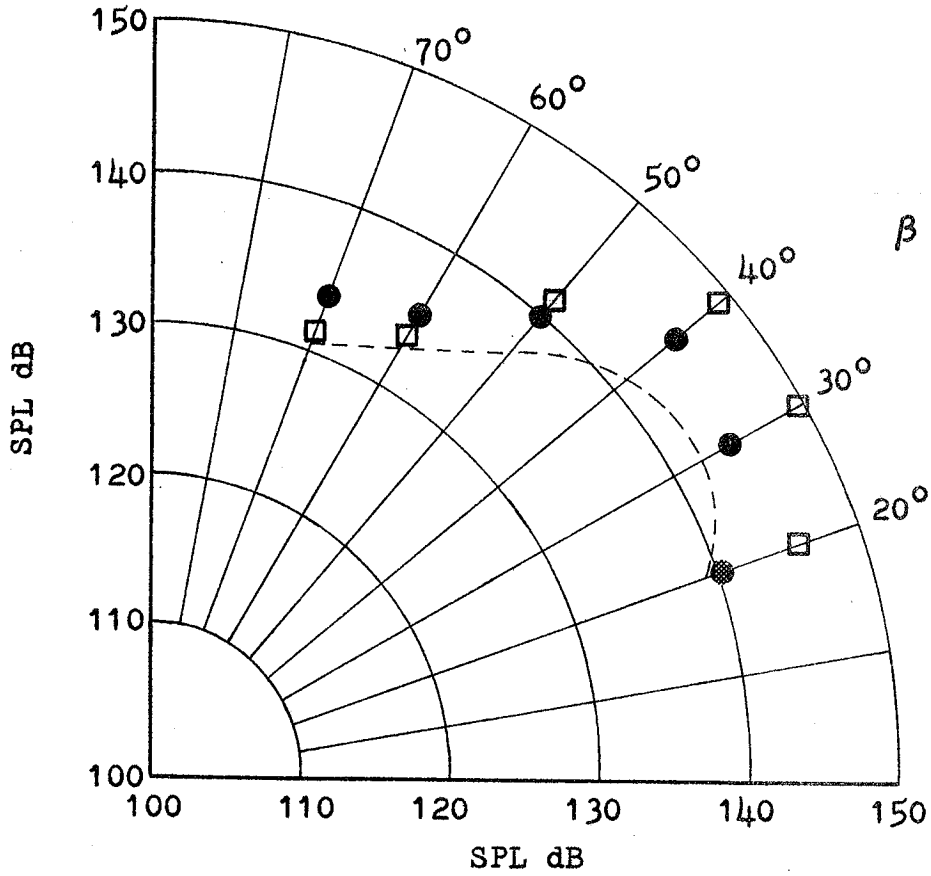

Figure 26. St=0.22 Total Sound Pressure Level Directivity Distribution, M=2.1, Perfectly Expanded Jet, R/D=30

□ - Glows In Phase

● - Glows Out Of Phase

(---)- Natural Jet

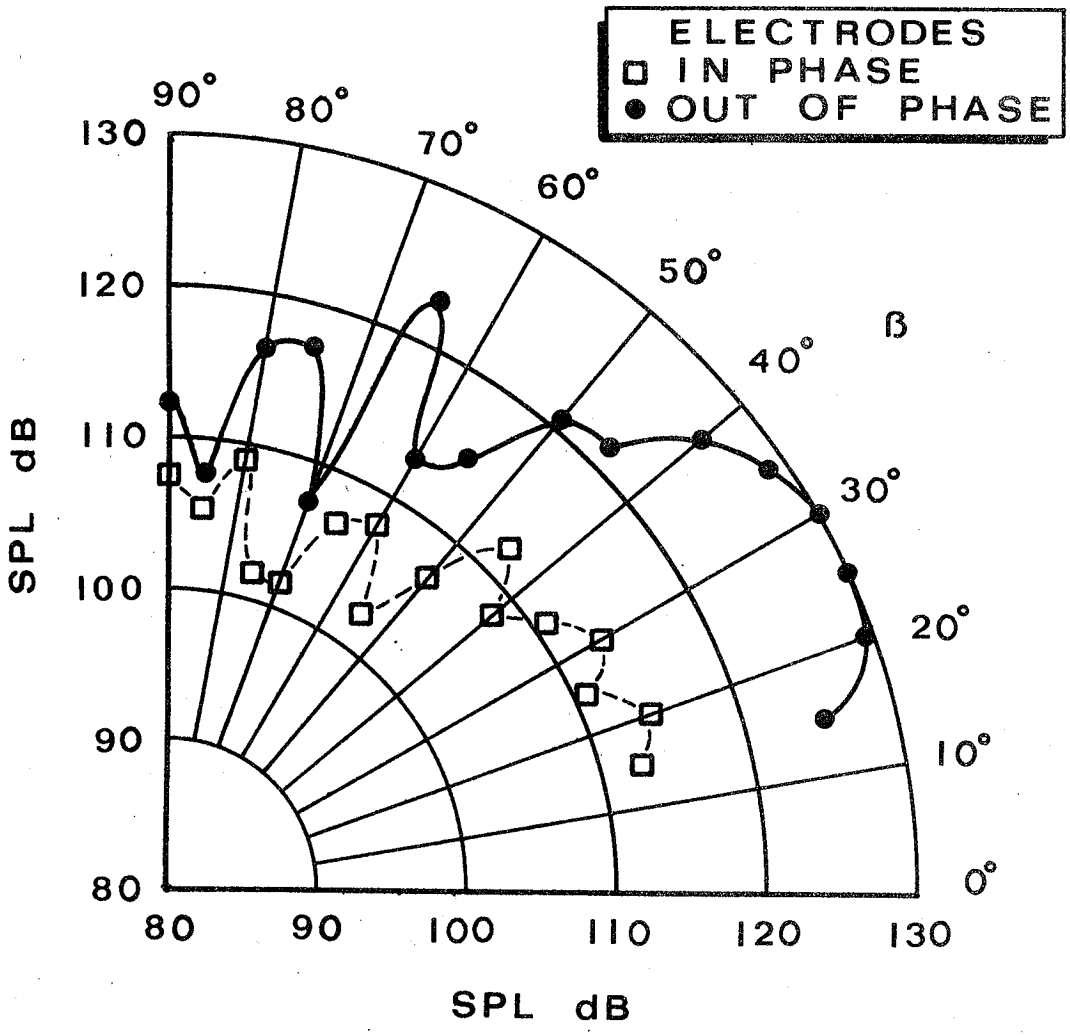

Figure 27. St=0.37 Coherent Sound Pressure Level Directivity Distributions, M=1.4 Underexpanded Jet, R/D=30, From Hu (10)

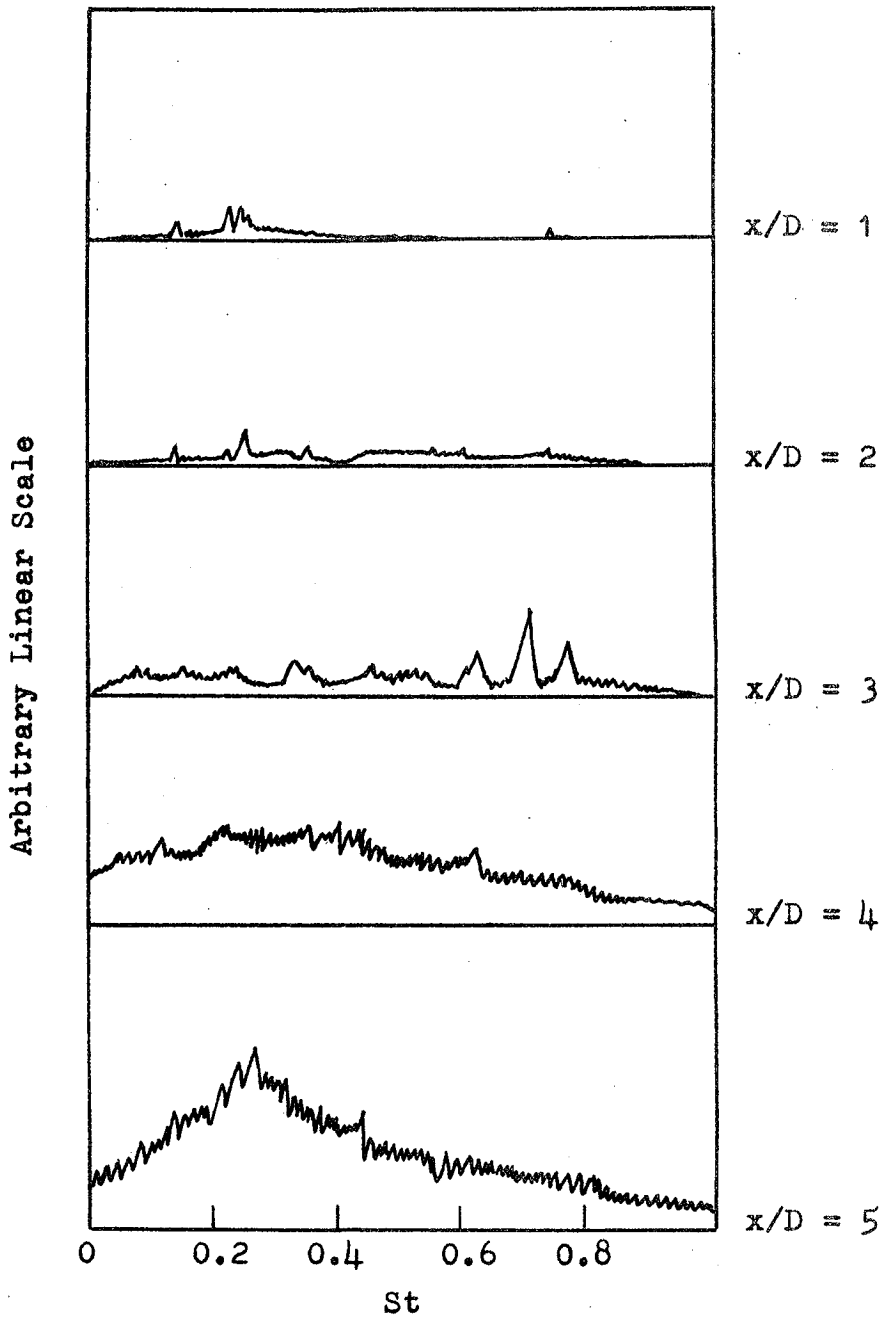

Figure 28. Hot-Wire Spectra on the Jet Centerline, Laminar Boundary Layer

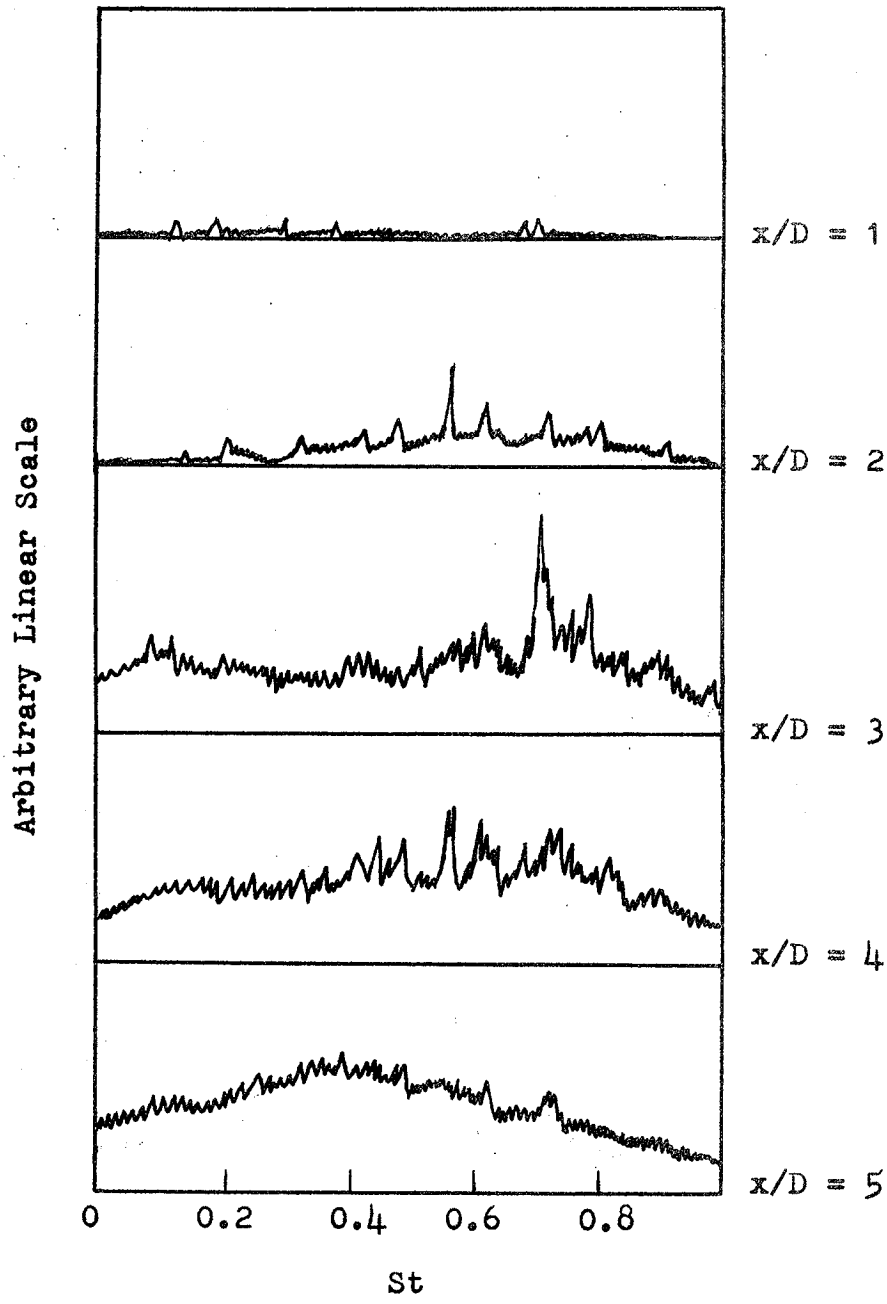

Figure 29. Hot-Wire Spectra in the Jet Shear Layer, Laminar Boundary Layer

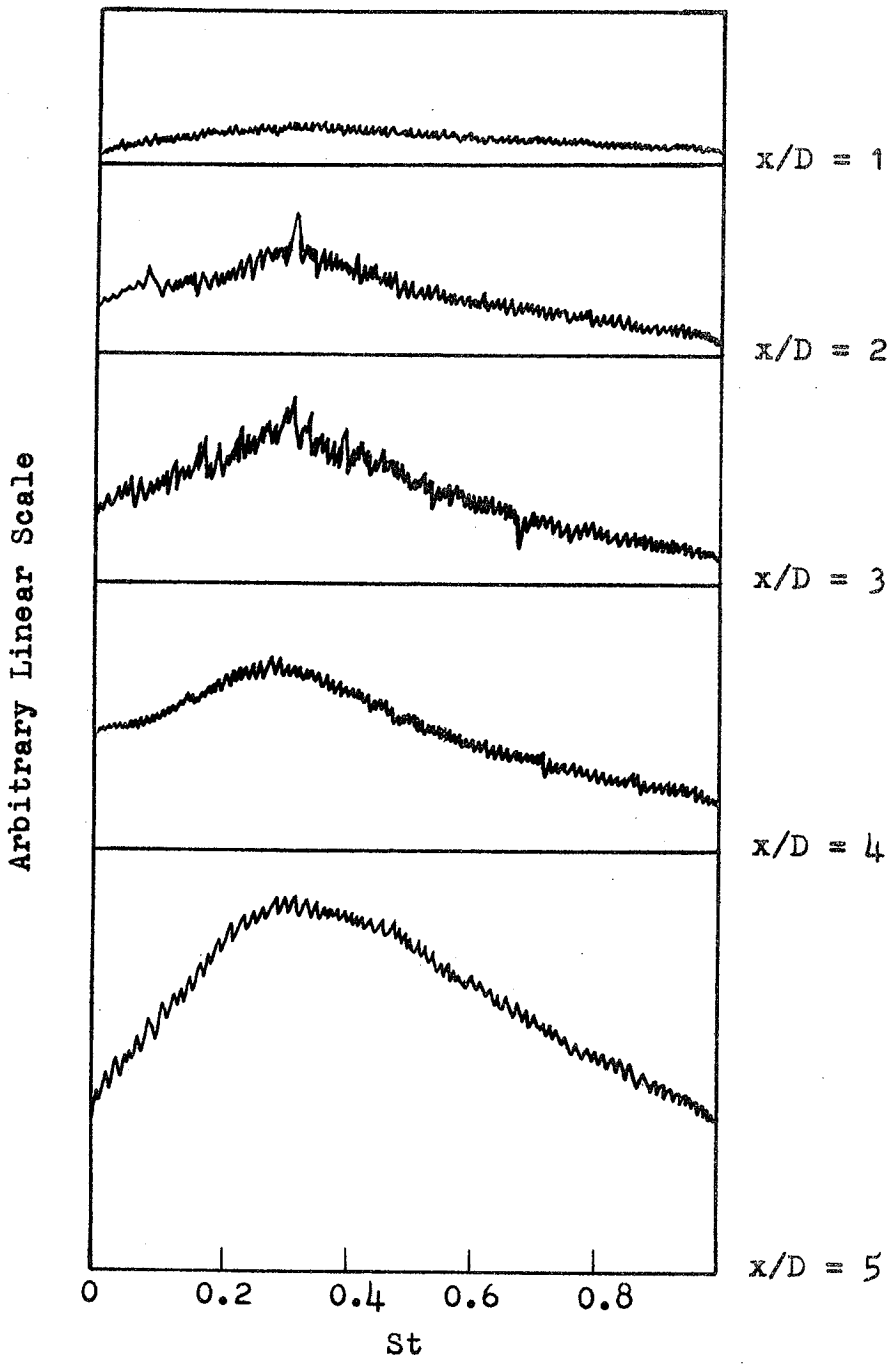

Figure 30. Hot-Wire Spectra on the Jet Centerline, Excited Boundary Layer

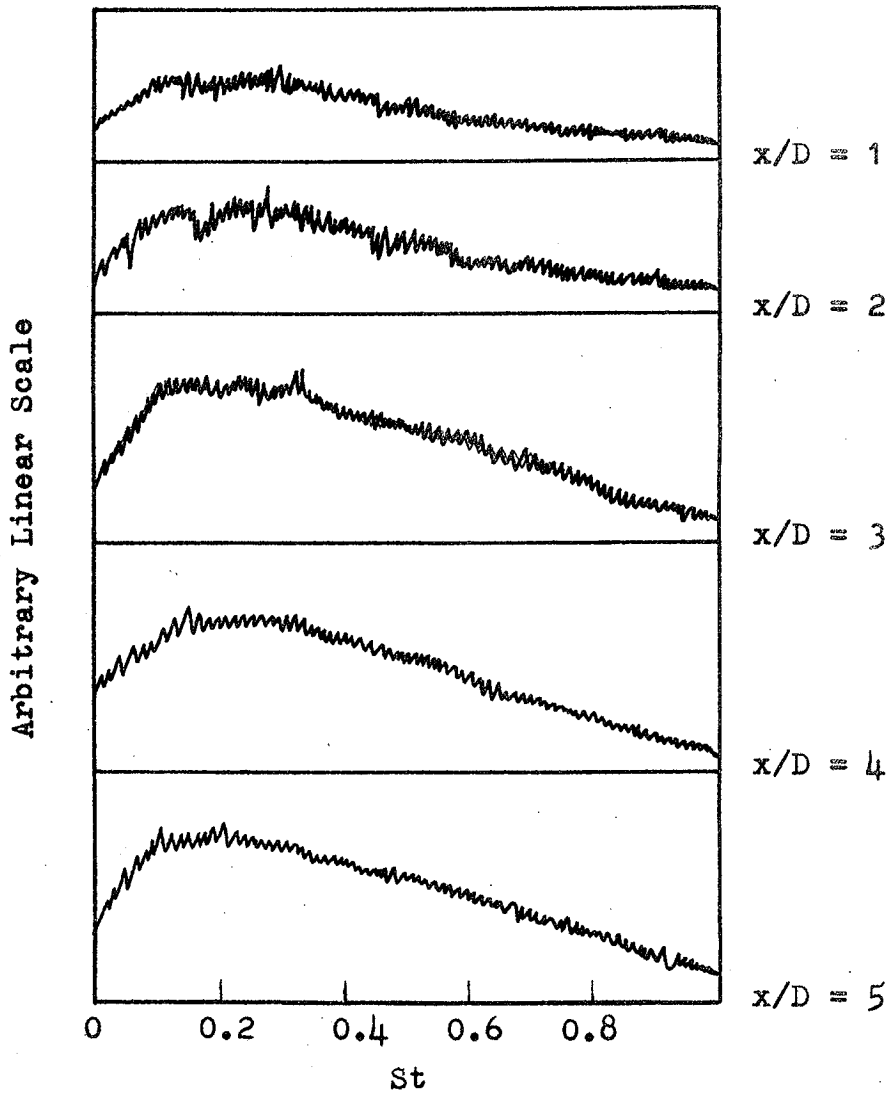

Figure 31. Hot-Wire Spectra in the Jet Shear Layer, Excited Boundary Layer

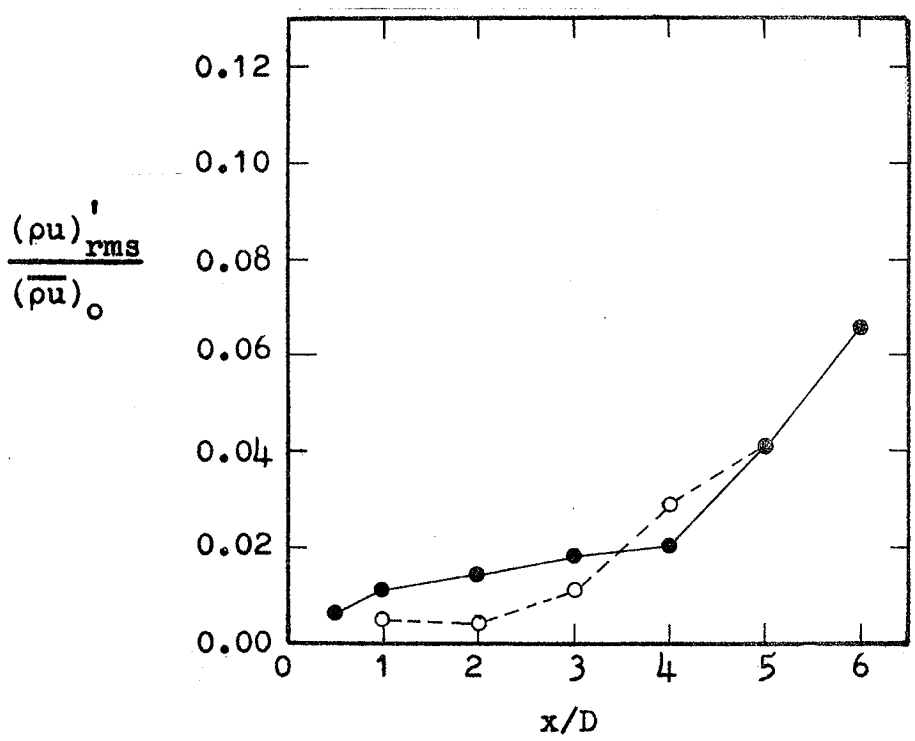

Figure 32. Overall Mass-Velocity Fluctuation Amplitude on the Jet Centerline

●—● - Excited Boundary Layer

○···○ - Laminar Boundary Layer

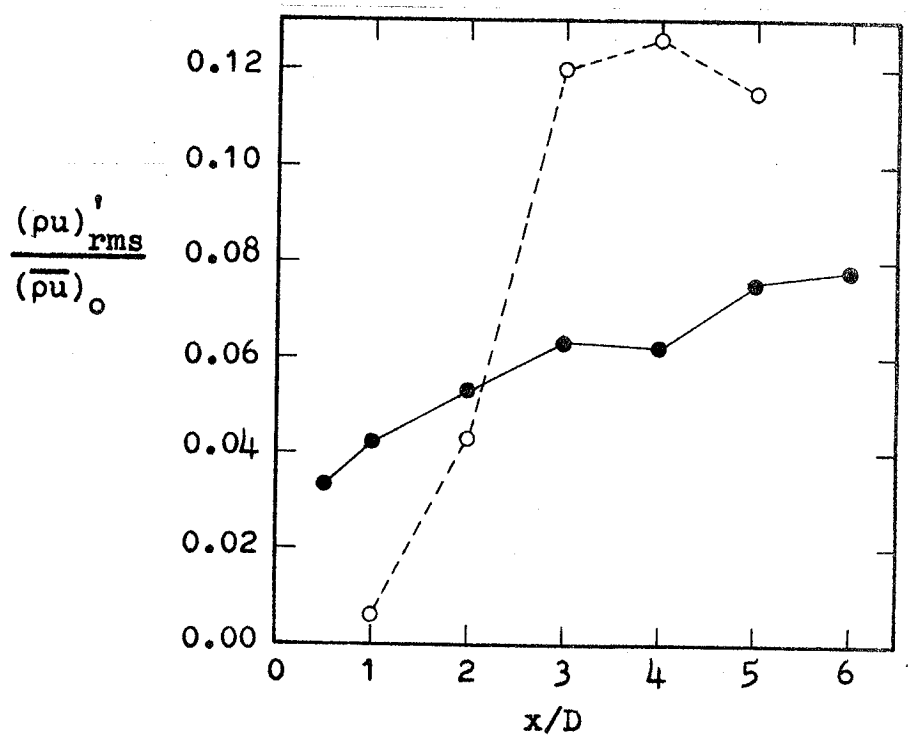

Figure 33. Overall Mass-Velocity Fluctuation Amplitude in the Jet Shear Layer

●—● - Excited Boundary Layer

○--○ - Laminar Boundary Layer

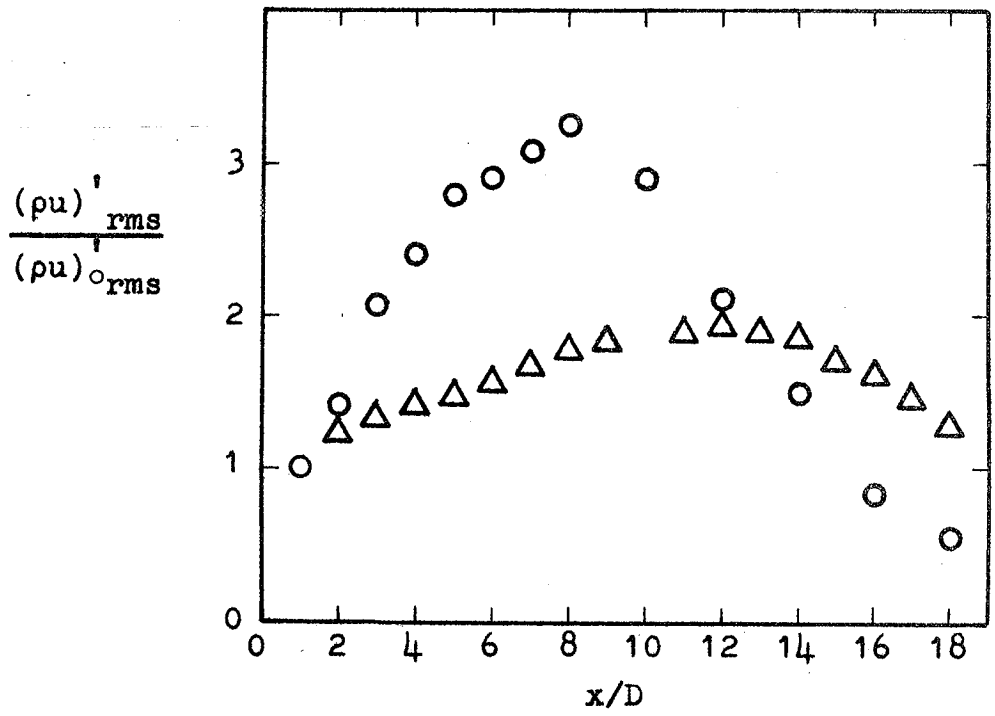

Figure 34. Bandpassed Mass-Velocity Fluctuation Amplitude in the Jet Shear Layer, St=0.20, Excited Boundary Layer

○ - Radial Location Point of Maximum Bandpassed Signal

△ - Constant Radial Location Along Nozzle Lip Line

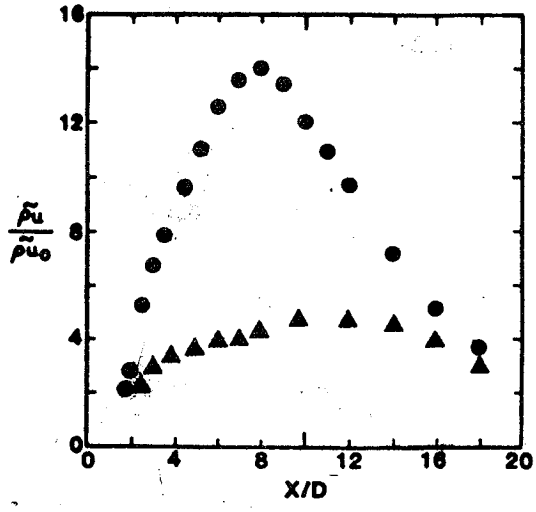

Figure 35. Bandpassed Mass-Velocity Fluctuation Amplitude in the Jet Shear Layer, St=0.20, From McLaughlin et al. (3)

- ● - M=2.1, Re=68,000 Jet, Hot-Wire Probe Used, Probe Position in Middle of Shear Layer
- ▲ - M=2.0, Re=5×10^6 Jet, Hot-Film Probe Used, Probe Position Along Nozzle Lip Line

Attachment #2

AN EVALUATION OF THE NOISE RADIATION CALCULATION OF THE COMPUTER CODE LSNOIS

M. S. Report

by

Lee-Fen Ko

ABSTRACT

The LSNOIS computer code developed by Morris and Tam calculates large scale instability wave evolution and the noise they radiate in supersonic jets. In its present form this code does a fair job of predicting both instability wave evolution and the resulting radiated noise. A study of the predictive ability of the near field part of the computation of the LSNOIS computer code was performed by inserting the experimental instability wave evolutions in place of the instability theory predictions. The calculation continued to produce near field sound predictions that were only in fair agreement with measurements. However, inclusion of both amplitude and phase instability data from experiment (for one jet condition) produced predictions of the near field in very good agreement with the measured near field.

The problems of numerical oscillations in the near field sound pressure level are found to be related to the step sizes of the axial distances or the wave numbers. Decreasing the step size in the wavenumber and/or increasing the total number of intervals reduces the problem of numerical oscillations.

The present calculations, performed with the LSNOIS computer code, demonstrate that the radiated noise calculation for specified large scale instabilities is surprisingly accurate. This theory, developed by Morris and Tam, represents a significant accomplishment in the field of aerodynamic noise, especially in light of the fact that a minimum of 'adjustable' constants are involved in the calculation.

TABLE OF CONTENTS

I. INTRODUCTION

Morris and Tam [1] developed a method for calculating the sound pressure generated by large-scale instabilities in axisymmetric jets. The method consists of two parts: (1) a calculation of the instability wave evolution in response to the mean flow development and other flow parameters, and (2) a radiated noise calculation using the wave evolutions obtained in the first part. The computer code produced for these calculations is documented in Tester, Morris, Lau and Tanna [2], and is called LSNOIS. McLaughlin, Seiner and Liu [3] evaluated the capability of LSNOIS to predict the results of experiments. For a wide range of experimental conditions, the instability evolutions and the near field sound pressure level were measured and compared with LSNOIS predictions. The body of experimental data consists of pitot and static pressure probe measurements of the mean flow velocities, hot-wire or hot-film probe measurements of the root-mean-square fluctuations of mass velocity in the flowfield and microphone measurements of the near field sound pressure level. These data were reported in Morrison and McLaughlin [4] for low Reynolds number jet conditions, Troutt and McLaughlin [5] for moderate Reynolds number jet conditions, and McLaughlin, Seiner and Liu [3] for high Reynolds number jet conditions. The comparison of the instability evolution provides a strict evaluation of the first part of calculation of the theory. A quantitative evaluation of the second part of the theory can be accomplished by using the experimental data for instability evolution as an intermediate input to the computer code. This has not been done and is the goal of the present work.

II. SUMMARY OF MORRIS-TAM ANALYSIS

2.1 Flow Field Instability Analysis

The instability process in cylindrical coordinates for a compressible, inviscid fluid is governed by the following set of linear disburbance equations:

$$\frac{\partial \rho'}{\partial t} + \frac{\partial}{\partial x_i}\left(\bar{\rho} u_i' + \rho' \bar{u}_i\right) = 0 \tag{1}$$

$$\gamma M_o^2 \left[\frac{\partial u_i'}{\partial t} + \bar{u}_j \frac{\partial u_i'}{\partial x_j} + u_j' \frac{\partial \bar{u}_i}{\partial x_j}\right] = -\frac{\partial P'}{\partial x_i} \tag{2}$$

$$\frac{\partial T'}{\partial t} + \bar{u}_j \frac{\partial T'}{\partial x_j} + u_j' \frac{\partial \bar{T}}{\partial x_j} + \gamma\left[\bar{T}\frac{\partial u_j'}{\partial x_j} + T'\frac{\partial \bar{u}_j}{\partial x_j}\right] = 0 \tag{3}$$

$$P' = \bar{\rho} T' + \rho' \bar{T} \quad , \tag{4}$$

where primes denote fluctuating quantities and bars denote mean flow quantities. M_o is the ratio of jet exit velocity to the ambient speed of sound and γ is the ratio of specific heats. Length, velocity and time, x_i, u_i and t, are nondimensionalized with respect to R_J, the radius of the jet at the nozzle exit, U_J, the exit velocity and R_J/U_J, respectively. The thermodynamic variables ρ, P and T, the density, pressure and temperature are nondimensionalzed with respect to corresponding ambient values. A slow variable, $s = \varepsilon x$, where the small parameter ε is a measure of the rate of spreading of the jet, is introduced to take into account of the slow divergence of the mean flow and the mean flow velocities and density are written:

$$\overline{u} = u_0(r,s)$$
$$\overline{v} = \varepsilon V_1(r,s) \quad .$$
$$\overline{\rho} = R_0(r,s)$$

A solution to equations (1) to (4) is of the form:

$$P'(r,\phi,x,t) = \hat{P}(r,s)\, e^{i\theta(x)+in\phi-i\omega t}$$

$$\rho'(r,\phi,x,t) = \hat{\rho}(r,s)\, e^{i\theta(x)+in\phi-i\omega t}$$

$$u'(r,\phi,x,t) = \hat{u}(r,s)\, e^{i\theta(x)+in\phi-i\omega t} \quad ,$$

where $n = 0,1,2,\ldots$ is the aximuthal wave number and ω is the frequency of the wave. The phase function $\theta(x)$ is such that

$$\frac{d\theta}{dx} = \alpha(s) \quad .$$

The complex amplitude distribution of the fluctuations is expanded in an asymptotic series of the form:

$$\hat{P}(r,s) = \hat{P}_0(r,s) + \varepsilon\hat{P}_1(r,s) + \varepsilon^2\hat{P}_2(r,s) \ldots$$

After substitution into equation (1) to (4) and some algebraic manipulations, a single equation for $\hat{P}_0$ is derived to order unity in ε.

$$\frac{\partial}{\partial r}\left(\frac{r}{R_0\Omega^2}\frac{\partial\hat{P}_0}{\partial r}\right) + \frac{r}{R_0\Omega^2}\left[M_0^2\Omega^2R_0 - \alpha^2 - \frac{n^2}{r^2}\right]\hat{P}_0 = 0 \qquad (5)$$

where $\Omega = \omega - u_0\alpha$. The boundary conditions are that $\hat{P}_0$ is bounded as $r \to \infty$ and $r \to 0$. Equation (5) and the boundary conditions form an eigenvalue problem. The eigenvalue is $\alpha = \alpha_r + i\alpha_i$ since ω, the frequency,

is taken to be real in a spatial stability formulation. The corresponding eigenfunction $\hat{P}_0$ has an arbitrary amplitude A(s), but A(s) is set equal to 1 for approximately parallel flow in the computer code LSNOIS.

2.2 Near Field Sound Calculation

The near field pressure fluctuations are calculated by a matched asymptotic expansion of the pressure field in the jet flow and the pressure field in the acoustic field. The result is

$$P'(r,\phi,x,t) = \left[\int_{-\infty}^{\infty} B_n(k) H_n^{(1)} \left(\sqrt{M_0^2\omega^2 - k^2}\, r\right) e^{ikx} dk \right] e^{in\phi - i\omega t} \qquad (6)$$

where $H_n^{(1)}$ is the nth order Hankel function of the first kind, and

$$B_n(k) = \frac{(M_0^2\omega^2 - k^2)^{n/2}}{2\pi} \int_{-\infty}^{\infty} \frac{e^{i\theta(x) - ikx}}{[M_0^2\omega^2 - \alpha(\varepsilon x)]^{n/2}} dx \quad , \quad n = 0,1,2,\ldots \qquad (7)$$

The sound pressure level in decibels is:

$$SPL(r,x) = 20 \log_{10} \left(\frac{P'_{rms}}{P_{ref}}\right) , \qquad (8)$$

where $P'_{rms} = |P'|$ and $P_{ref} = 2 \times 10^{-5}$ N/m^2 x $\left(\frac{p_c}{p_a}\right)$. p_a is standard atmospheric pressure and p_c is the pressure of the test chamber into which the jet exhausts.

III. DESCRIPTION OF MODIFICATION TO CODE

3.1 Background

Mean velocity profiles in the code are represented as a half-Gaussian of the form:

$$\frac{\overline{u}(\eta)}{U} = \exp[-2.773\ (\eta+0.5)^2] \qquad \text{for } \eta > -0.5$$
$$= 1 \qquad \text{for } \eta \leq -0.5 \tag{9}$$

where $\eta = (r-r(.5))/\delta$, U is the velocity on the centerline of the jet at the given x-location, r(.5) is the radial location where the velocity equals 0.5U and δ is the local shear layer thickness. Experimental data are curve fit to the above half-Gaussian to obtain r(.5) and δ as function of axial distance. For example, the mean velocity profile parameters for the moderate Reynolds number jet are shown in Figure 1. The two parameters, r(.5) and δ, are input to the code to generate the mean velocity profile.

The instability wave is predicted to be of the form $Q(x,r,\phi,t) = \hat{Q}(r)\ \exp(i\theta(x) + in\phi - i\omega t)$ in the theory. The normalized hot-wire data of the root-mean-square mass velocity fluctuations correspond to the amplitude of the instability wave divided by the exit instability amplitude.

$$\left|\frac{Q(x,r,\phi,t)}{Q(0,r,\phi,t)}\right| = |\exp(i\theta(x))| \tag{10}$$

In Figure 2 an example is shown of the instability wave evolution of the St = 0.2 component for the moderate Reynolds number M = 2.1 jet,

where circles represent measured data and curves represent predictions from instability analysis for azimuthal numbers n = 1 and 0. Figure 3 shows the measured near field sound pressure level contours and the SPL taken from the predictions using the instability evolution data of Figure 2. The sound pressure level contours on the prediction plots do not have labeled SPL values. The reason for this is that there is one adjustable parameter in the calculated SPL field, namely the level at one point in the field, to which the relative sound level at all other points is referenced. In Figure 3, and subsequent figures showing predicted near fields, the calculated sound pressure level contours are 2 dB apart with the unspecified reference level.

The objective of the present study is to input measured instability amplitudes into the computer calculation and examine the calculated SPL data therefrom.

3.2 Code Modification

Modifications to the LSNOIS computer code were made in the DIRECT subroutine where the near field pressure is calculated. Two subroutines, ELDATA and EVOL were added to the existing DIRECT subroutine as shown in the block diagram of Figure 4. The relationship of the subroutine DIRECT to the full program LSNOIS is given in Tester *et al.* [2]. Figure 5 shows block diagrams of ELDATA and EVOL. The subroutine ELDATA has instability wave amplitude data for a number of jet conditions and spectral components stored in data arrays. Choice of the flag parameter IFLED either chooses the appropriate instability data that will replace previously

calculated data, or return without changing the theoretical instability data. (IFLED=0 leaves the theoretical data unchanged.)

The subroutine EVOL performs two functions. First, it performs a search and linear interpolation on the corresponding experimental instability amplitude which then is used to replace the theoretically calculated instability amplitude. Second, with the appropriate setting of IPHASE, the experimentally determined phase is input from a simple calculation with the constant wavenumber. A block diagram for EVOL is also shown in Figure 5. The modifications to the instability amplitude and phase data are normally checked by a write command for the instability evolution.

IV. RESULTS AND DISCUSSION

Calculations of the near field sound pressure level from experimentally determined wave evolutions were performed for two jet conditions, both having a nominal exit Mach number of 2. The case to be presented first is the M = 2.0, Re = 5.2 x 10^6 (conventional high Reynolds number) jet in which the measured wave evolution amplitude distribution is considerably different from the theoretical one [3]. The second case is the M = 2.1, Re = 70,000 (moderate Reynolds number) jet in which not only is the measured wave evolution amplitude distribution closer to the theoretical one, but also experimental data on the phase of individual spectral components have been obtained. Consequently, calculations on this jet can be performed which demonstrate the effect of using experimental phase information as well as instability wave amplitude information. In both jet conditions only data corresponding to the St = 0.2 mode are presented. Additional experimental and computational data at St = 0.4 have been obtained which are similar to the St = 0.2 data and, thus, for the sake of brevity, are not included in this report.

4.1 High Reynolds Number, M = 2.0 Jet Results

Figure 6 shows the measured amplitude of the wave evolution of the St = 0.2 component of the high Reynolds number, M = 2.0 jet (from Reference [2]). Also shown on the figure are the amplitude evolutions calculated by the LSNOIS code for modes n = 0 and n = 1. The large scale instability is made up of an unknown mixture of azimuthal modes. Measurements performed by Troutt and McLaughlin [5] in a similar moderate

Reynolds number jet suggest that the lower order modes predominate the instability. Consequently, calculations are performed here for the n = 0 and n = 1 azimuthal modes and the experimental data are presumed to approximate a mixture of the two lowest order modes. The high Reynolds number M = 2.0 jet case was chosen for the initial calculation because it is the one with the greatest discrepancy between the measured and predicted wave amplitude evolutions. Thus, it is reasonable to expect the predicted near field SPL contours to agree more closely with measured contours if the calculated wave evolution is replaced with the measured amplitude evolution. In Figures 7 and 8, the measured and predicted near field sound pressure level contours are presented for the mode numbers 0 and 1, St = 0.2 components, respectively. Part (a) of the figures shows the measured SPL contours, from Reference [3]. Part (b) presents the predicted SPL contours using the standard version of LSNOIS, which calculates the noise radiated from calculated instabilities. Part (c) presents predicted SPL contours using the modified version of LSNOIS which substitutes the measured instability amplitude evolution for the calculated one.

With the apparent differences in the input wave evolutions in Figure 6, the near fields turn out to be unexpectedly similar. Compared to the measured near fields, little improvement is seen. In order to understand the results, the wavenumber spectra are also plotted in Figures 9 and 10, where the differences between spectra of experimental and theoretical evolutions occur mainly at large wavenumber values. These apparently anomalous results can be explained by analytical considerations using a

modeled instability evolution. This analysis is performed in the next section.

4.2 Analytical Considerations Related to the Near Field

The apparently anomalous behavior of the predicted near field sound pressure levels in relation to the instability amplitude evolution can be explained with some simple analytical considerations. The first issue addressed is: why do the differences in wavenumber spectra result in so little change in the near field?

Referring to equation (6):

$$P'(x,t) = \left[\int_{-\infty}^{\infty} B_n(k) H_n^{(1)} \left(\sqrt{M_o^2\omega^2 - k^2}\, r\right) e^{ikx} dx \right] e^{in\phi - i\omega t} \quad . \tag{6}$$

Examining the asymptotic form of the Hankel function (which is a good approximation for most radial locations at which the near field is evaluated).

$$H_n^{(1)}(z) \approx \sqrt{\frac{2}{\pi}} \frac{e^{iz - i\left(\frac{\pi}{4} + \frac{n\pi}{2}\right)}}{\sqrt{z}} \tag{11}$$

$$\left| B_n(k) H_n^{(1)} \left(\sqrt{M_o^2\omega^2 - k^2}\, r\right) \right| \approx \left| \frac{B_n^*(k)}{\pi\sqrt{2\pi\, r}} \sqrt{z}\, e^{iz - i\left(\frac{\pi}{4} + \frac{n\pi}{2}\right)} \right|$$

$$= \frac{\left|B_n^*(k)\right|}{\pi\sqrt{2\pi\, r}} \left|\sqrt{z}\right| e^{-z_i} \quad , \tag{12}$$

where

$$z = \sqrt{M_0^2\omega^2-k^2}\, r, \quad B_n^*(k) = \frac{2}{\pi\sqrt{M_0^2\omega^2-k^2}} B_n(k)$$

$$M_0^2\omega^2 = 0.086, \quad r = 6, 12, 18, 24, \ldots$$

Thus, the amplitude of the Fourier integrand decays like $\sqrt{k/r}\, e^{-rk}$ and essentially only those wavenumber components with small k are significant. So the differences in wavenumber spectra between experiment and theory, which are mainly in the large k range, are lost when multiplied by the Hankel function.

The second issue addressed is: why does the difference in wave evolution not result in more significant differences in the location and the width of the peak in the wavenumber spectra?

The wavenumber spectra plotted in Figures 9 and 10

$$B_n^*(k) = \int_{-\infty}^{\infty} \frac{e^{i\theta(x)-ikx}}{[M^2\omega^2-\alpha^2]^{n-2}}\, dx \tag{13}$$

is essentially a Fourier transform of the instability wave evolution. The amplitude of both theoretical and experimental wave evolutions can be approximated by a Gaussian shape, whose Fourier transform is known analytically. Let $G_\xi(x)$ be a Gaussian function with a half width ξ, a peak at $x = 0$, and k_0 and x_0 real constants. Therefore, $G_\xi(x-x_0)$ will represent the amplitude of the wave evolution peaking at x_0 and k_0x will represent the phase of the wave evolution. From Fourier analysis [6]:

$$F[G_\xi(x)] = \xi G_{1/\xi}(k)$$

$$F[G_\xi(x-x_o)] = \xi G_{1/\xi}(k)\, e^{-ix_o k} \tag{14}$$

$$F[G_\xi(x-x_o)\, e^{ik_o x}] = \xi G_{1/\xi}(k-k_o)\, e^{-ix_o k}$$

where $F[\ ]$ stands for the Fourier transform of $[\ ]$. Thus, the position of the peak of the wavenumber spectrum, k_o in $G_{1/\xi}(k-k_o)$, is mainly determined by the phase of the wave evolution rather than the amplitude. Since the phase of the experimental wave evolution was set equal to that of the theoretical wave evolution for lack of experimental phase data, their spectra peak at about the same position.

Another problem is that the half width of the spectra, ξ, is about equal in Figures 9 and 10 rather than being inversely proportional to the half width of the wave evolution as is predicted by Fourier analysis and comparison of Figures 6, 9 and 10. The reason for this is that the above analysis treats k_o as constant. However, the actual k_o varies with distance. The more spread-out wave evolution takes in more variation of k_o, and tends to spread out the wavenumber spectra and cancel the narrowing due to the amplitude of wave evolution.

In summary, this analysis demonstrates the importance of using empirical phase, as well as amplitude, information in a definitive evaluation of the near field predictive capability of the Morris-Tam noise radiation calculation method.

4.3 Moderate Reynolds Number, M = 2.1 Jet Results

In the last section it was demonstrated that the instability phase information is as important as the amplitude data, in the calculation of the radiated noise. Therefore, comparisons of predicted noise radiation from a moderate Reynolds number, M = 2.1 jet are very important in this LSNOIS computer code evaluation. In the case of the moderate Reynolds number jet, phase information of specific spectral components in the jet is available because of the unique circumstances of the moderate Re experiments (Reference [5]). Consequently, calculations of the radiated noise (using LSNOIS) can be accomplished with empirical amplitude and phase data, and compared with the measured sound field.

Figure 11 presents calculated near field sound pressure level contours for the St = 0.2 component of the moderate Reynolds number M = 2.1 jet. As in Figure 3, Part (a) presents the experimental data and Parts (b) and (c) present the calculations for the n = 0 and n = 1 modes, respectively. Figure 3 presents calculated SPL contours with theoretically calculated instability evolutions. Figure 11, on the other hand, presents calculated SPL contours using measured instability amplitude evolution and phase data. The amplitude data for this jet condition are depicted in Figure 2, while the phase distribution was measured by Troutt and McLaughlin [5] to be linearly varying with axial distance, and having an approximately constant wavenumber $k_r D = 1.6$.

It is apparent that a sound field made up of a combination of the calculated n = 0 and n = 1 fields is in reasonable agreement with the

experimental measurements and a noticeable improvement has been made over the calculations shown in Figure 3. The most noticeable feature is the directivity of the dominant noise emission falling closer to the jet axis. This, and the data like it for the St = 0.4 mode, attest to the validity of the noise radiation prediction ability of the LSNOIS computer code.

4.4 Numerical Oscillations

The numerical resolution of the computer code LSNOIS is determined by two pararmeters, dx and dk (DELX and DW in FORTRAN nomenclature). DELX is set equal to $0.5/\pi St$ in LSNOIS while DW is set to 2π/DELX*INUM, where INUM is a parameter which determines the number of steps in the wavenumber space. Therefore, the product DELX*DW = 2π/INUM and is typically held constant during several parametric computer runs.

The resolution of the wave evolution is determined by DELX while DW controls the resolution of the wavenumber spectrum. Since the wavenumber spectrum usually has a narrow peak, there are often numerical oscillations apparent in the near field data caused by inadequate wavenumber resolution. Such oscillations are normally more prevalent in the higher frequency spectral components.

An example of apparent numerical oscillations is shown in Figure 12 which depicts predicted near field SPL contours for the St = 0.4 component of the moderate Reynolds number M = 2.1 jet. In part (b) of the figure the result for dx = DELX and kd = DW is shown, as specified in the

regular version of LSNOIS. Parts (a) and (c) have modifications made to the step sizes as follows: (a) dx = 0.5 DELX, dk = 2.0 DW and (c) dx = 1.5 DELX and dk = 0.67 DW. Noticeable oscillations in the near field data under normal operation are smoothed by increasing the wavenumber resolution at the expense of dx resolution as in part (c). The oscillations are exacerbated when the dx resolution is improved at the expense of the wavenumber resolution.

A more reliable way of decreasing the oscillations in the near field data is to decrease the wavenumber step size without altering the dx step size. To do this, the total number of intervals must be increased (by increasing INUM). An example of such a computation is shown in Figure 13 where dx = DELX and dk = 0.5 DW were specified. Of course, increasing the number of intervals increases the computational expense.

These computations have demonstrated that numerical oscillations in the near field calculations can be controlled by appropriate choices of step sizes of the axial coordinate x and the wavenumber k.

V. CONCLUSIONS

The radiated noise calculation in the LSNOIS computer code, using measured flowfield instability amplitude and phase data, produces predictions that are in very good agreement with microphone measurements (for the moderate Reynolds number M = 2.1 jet). Replacing only the amplitude distribution of the instability with measured data does not significantly improve the calculation's agreement with near field SPL measurements. Consequently, the instability phase information plays at least as important a role, if not a more important role, in the accurate calculation of the sound field (using LSNOIS).

The problems of numerical oscillations in the near field SPL are found to be related to the step sizes of the wavenumber or axial distance. Decreasing the step size in the wavenumber and/or increasing the total number of intervals reduces the problem of numerical oscillations.

NOMENCLATURE

A	Amplitude of $\hat{P}$
B_n	$B_n^*(M_o^2\omega^2-k^2)^{n/2}/2\pi$
B_n^*	Wavenumber component
D	Jet nozzle exit diameter
dx	Step size of axial distance in code
dk	Step size of wavenumber in code
G_ξ	Gaussian function with half width ξ
$H_n^{(1)}$	Hankel function of the first kind
k	Wavenumber
k_o	Approximate phase of instability wave evolution
M	Jet Mach number
M_o	Ratio of jet exit velocity to ambient speed of sound
n	Azimuthal mode number
p	Pressure
P_{rms}	$\lvert P' \rvert$
P_{ref}	$2 \times 10^{-5} N/m^2 \times (p_c/p_a)$
Q	A typical flow quantity
r,R	Radial coordinate
R_e	Jet Reynolds number based on exit conditions = $\rho_e U_e D/\mu_e$
R_j	Radius of jet at nozzle exit
R_o	Measured mean density
s	εx
S_t	Strouhal number = fD/U
t	Time
T	Temperature

u	Velocity (x-component)
U_o	Measured mean velocity (x-component)
U	Jet centerline velocity
v	Velocity (y-component)
v_1	Measured mean velocity (v component)
x	Axial coordinate
x_o	Approximate location of peak of instability wave evolution amplitude
z	$\int_o^x \sqrt{M_o^2\omega^2-k^2}\, r$
α	$\int_o^x k\, dx'$
γ	Ratio of specific heats
ϕ	Jet shear layer thickness
ε	Small parameter; rate of shear layer spread
ρ	Density
θ	$\int_o^x \alpha\, dx$
ϕ	Azimuthal coordinate
ω	Angular frequency = $2\pi f$
Ω	$\omega - U_o\alpha$
η	$(r-r(.5))/\delta$
$(\bar{\ })$	Time average quantity
$(\ )'$	Fluctuating quantity
$(\tilde{\ })$	Root mean square of fluctuating quantity
$(\hat{\ })$	Amplitude envelope of fluctuations
$(\hat{\ })_n$	nth order quantity in asymptotic series of $(\hat{\ })$ quantity
$(\ )_e$	Jet exit condition
$(\ )_a$	Standard atmospheric condition
$(\ )_c$	Test chamber condition

REFERENCES

1. Morris, P.J. and Tam, C.K.W., *"Near and Far Field Noise From Large-Scale Instabilities of Axisymmetric Jets,"* AIAA Paper No. 77-1351, 1977.

2. Tester, B.J., Morris, P.J., Lau, J.C. and Tanna, H.K., *"The Generation, Radiation and Prediction of Supersonic Jet Noise - Volume 1,"* Technical Report AFAPL-TR-78-85, 1978.

3. McLaughlin, D.K., Seiner, J.M. and Liu, C.H., *"On the Noise Generated by Large-Scale Instabilities in Supersonic Jets,"* AIAA Paper No. 80-0964, 1980.

4. Morrison, G.L. and McLaughlin, D.K., *"Instability Process in Low Reynolds Number Supersonic Jets,"* AIAA Journal, 18, pp. 793-800, 1980.

5. Troutt, T.R. and McLaughlin, D.K., *"Experiments on the Flow and Acoustic Properties of a Moderate-Reynolds-Number Supersonic Jet,"* J. of Fluid Mech., 116, pp. 123-156, 1982.

6. Papoulis, A., The Fourier Integral and Its Applications, McGraw-Hill, 1962.

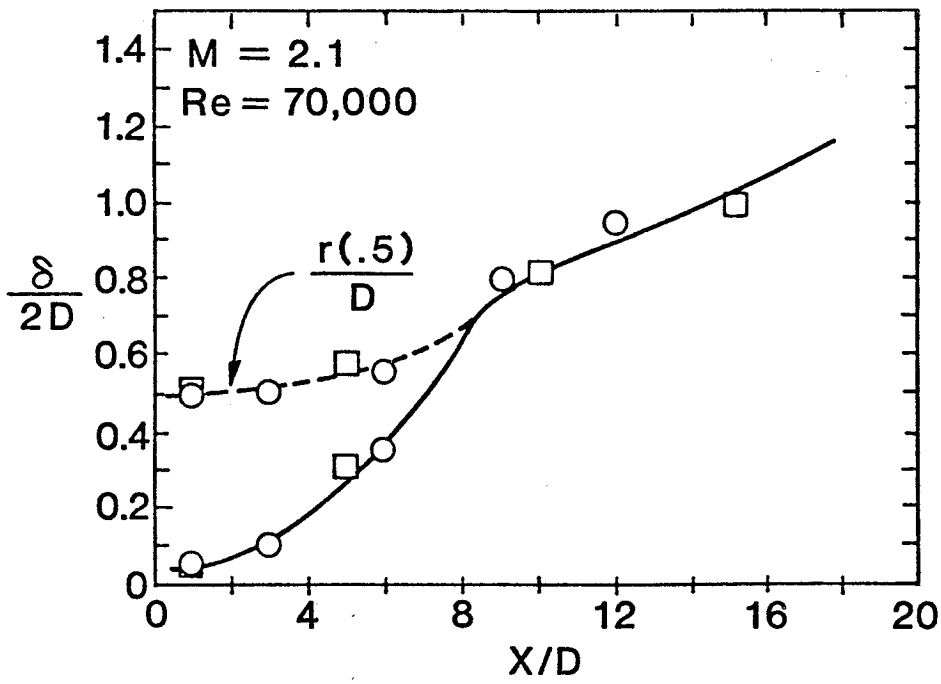

Figure 1. Axial Distribution of the Mean Velocity Profile Parameters for the M = 2.1, Re = 70,000 Jet [Ref. 5]

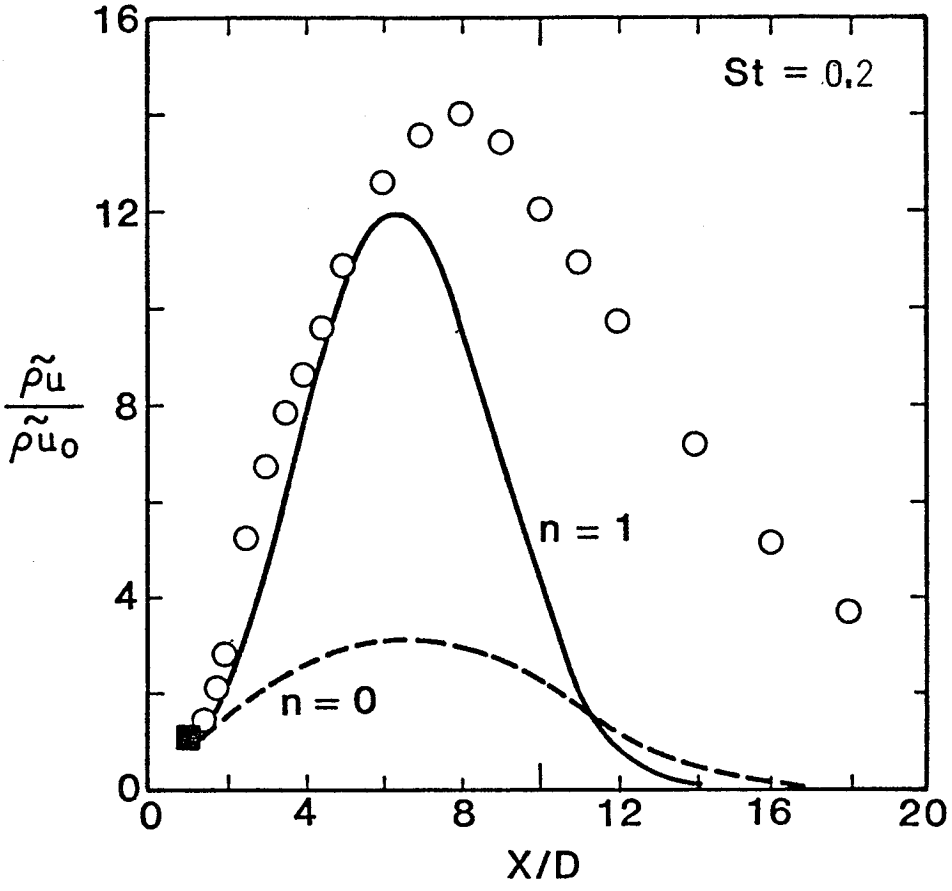

Figure 2. Axial Distributions of the Narrow Band Mass Velocity Fluctuation Amplitude in the Jet Shear Layer for the M = 2.1, Re = 70,000 Jet

○ Experiment [Ref. 5]. —— n = 1, ---- n = 0 prediction.

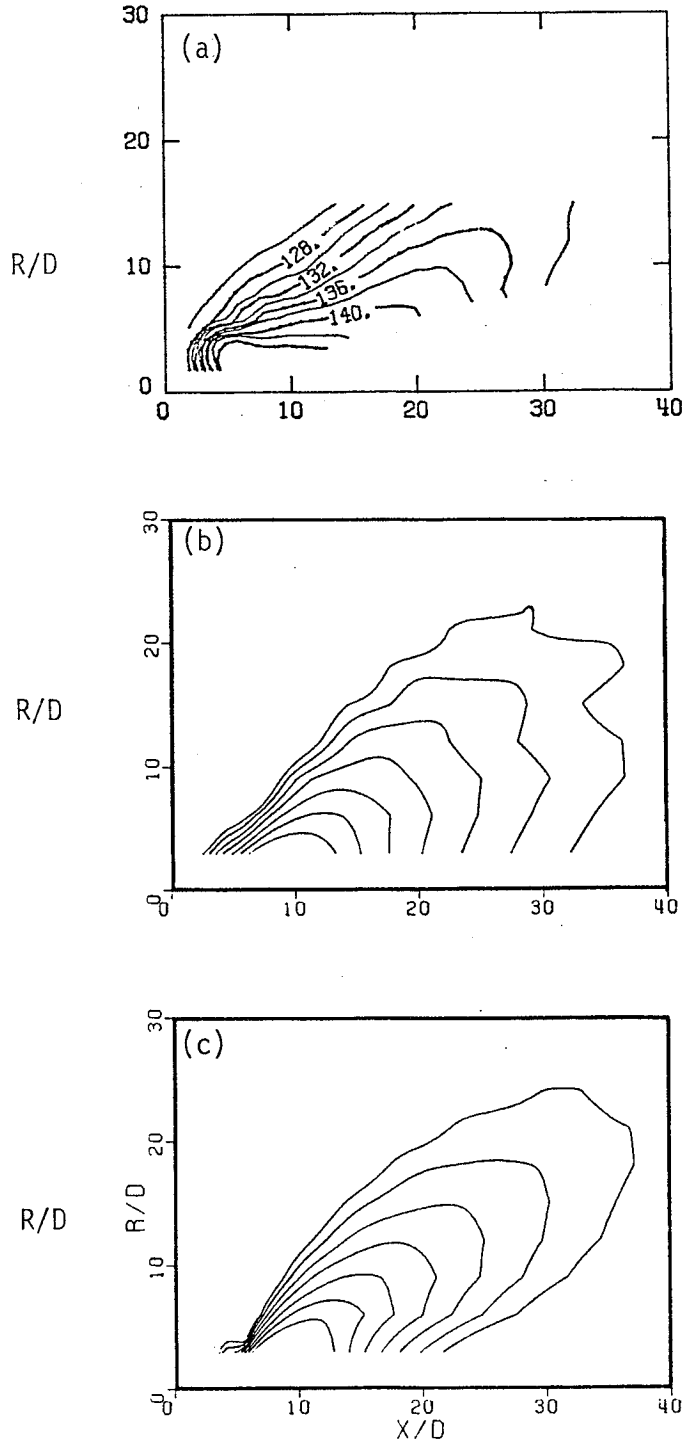

Figure 3. Band Passed Near Field Sound Pressure Level Contours for the St = 0.2 Component of the M = 2.1, Re = 70,000 Jet

(a) Experiment [Ref. 5]
(b) n = 0 prediction
(c) n = 1 prediction

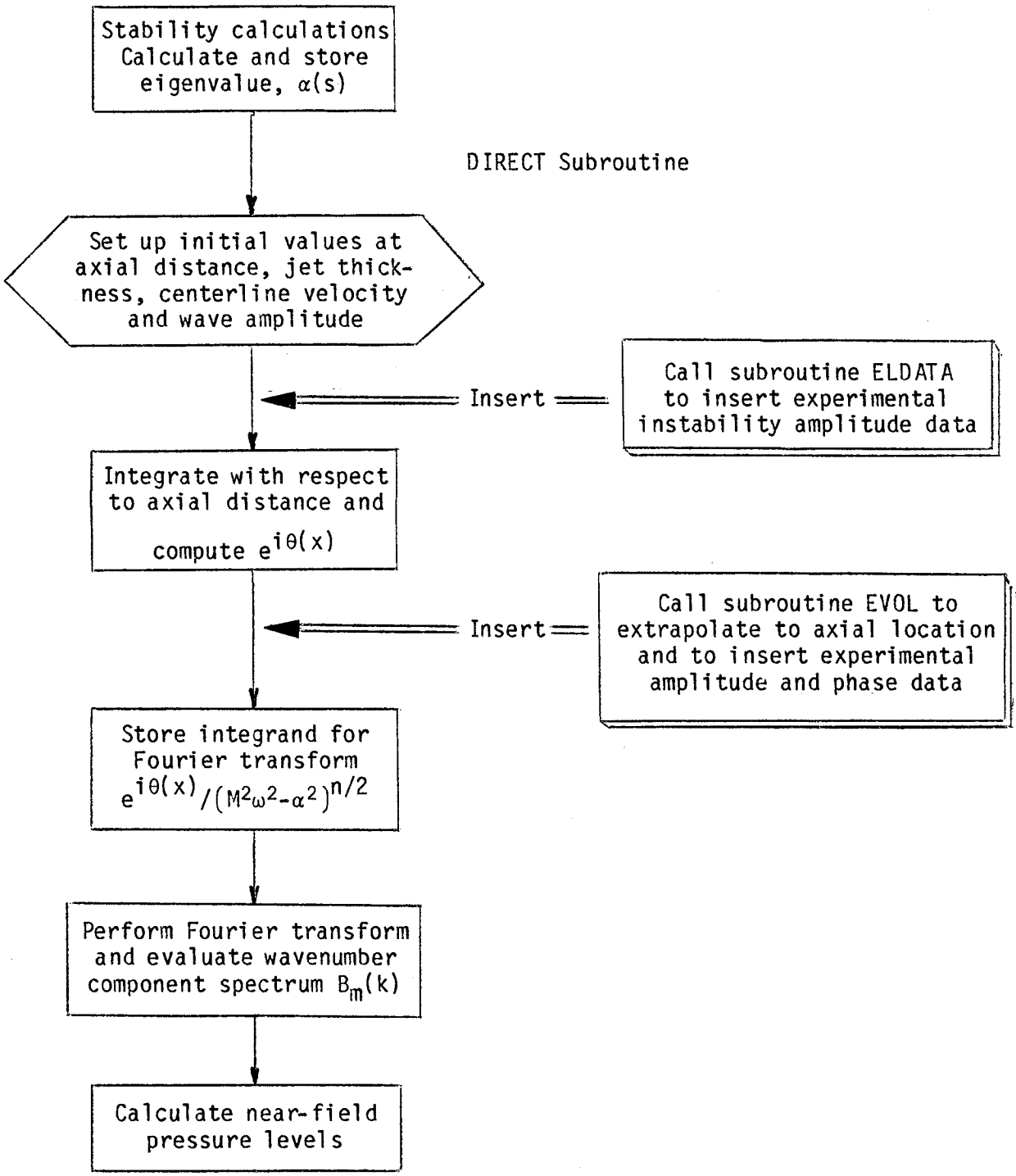

Figure 4. Block Diagram of Subroutine DIRECT With Modifications Specified

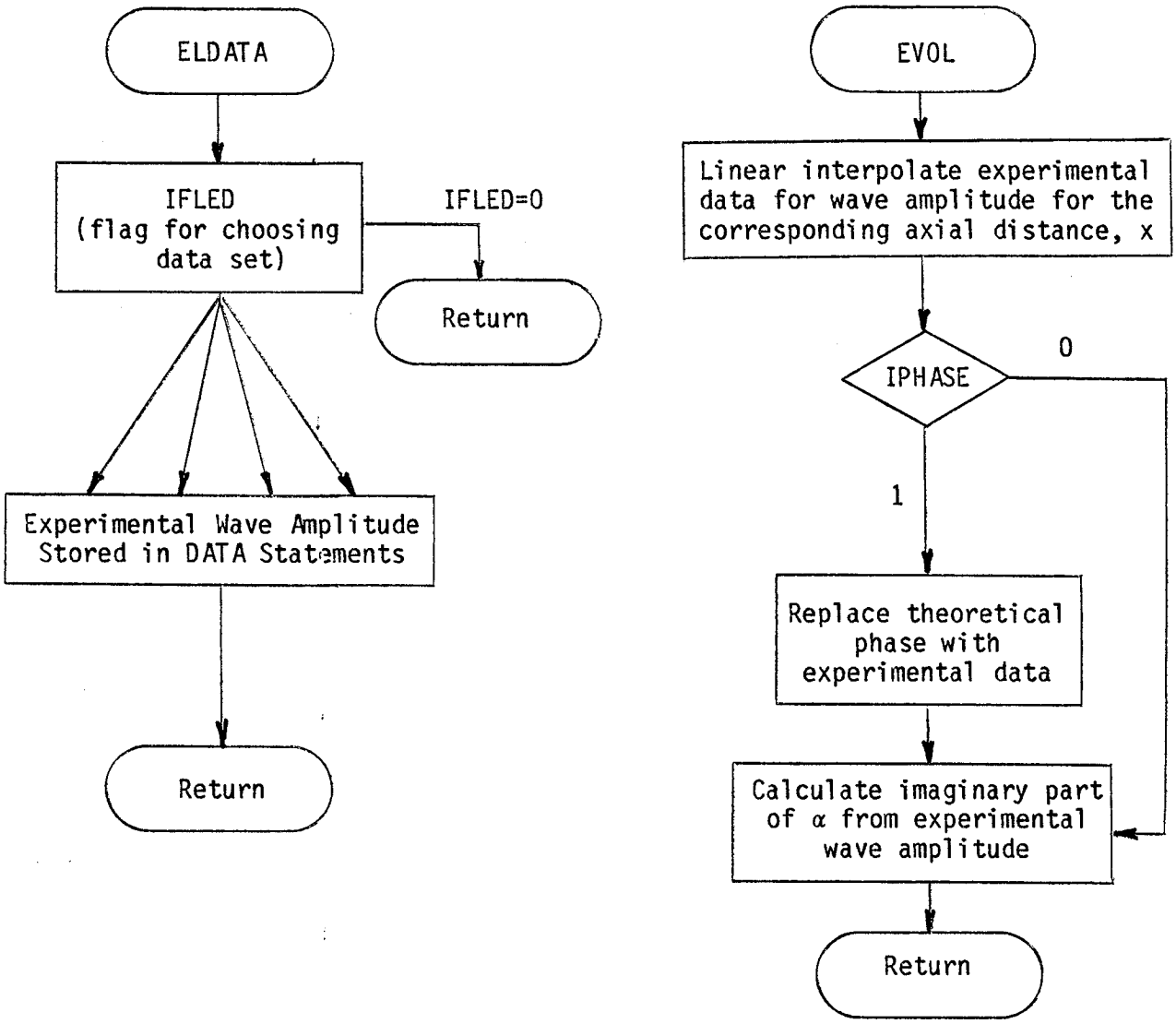

Figure 5. Block Diagrams of the New Subroutines ELDATA and EVOL

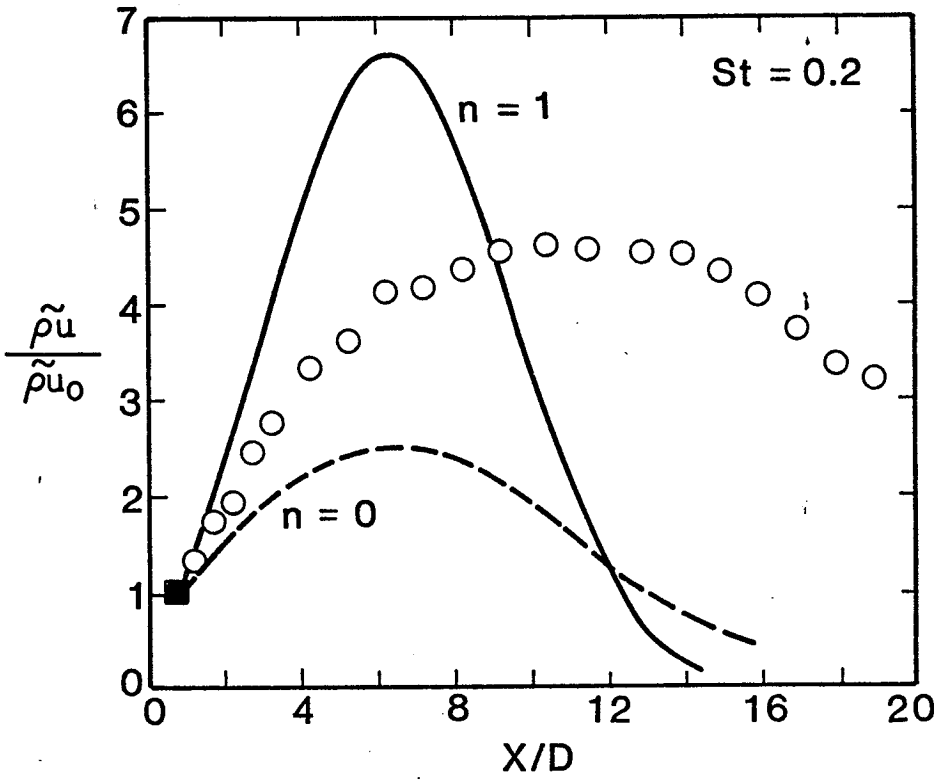

Figure 6. Axial Distribution of the Narrow Band Mass Velocity Fluctuation Amplitude in the Jet Shear Layer for the M = 2.0, Re = 5.2 x 10^6 Jet.

○ Experiment [Ref. 5], —— n = 1 prediction,
---- n = 0 prediction

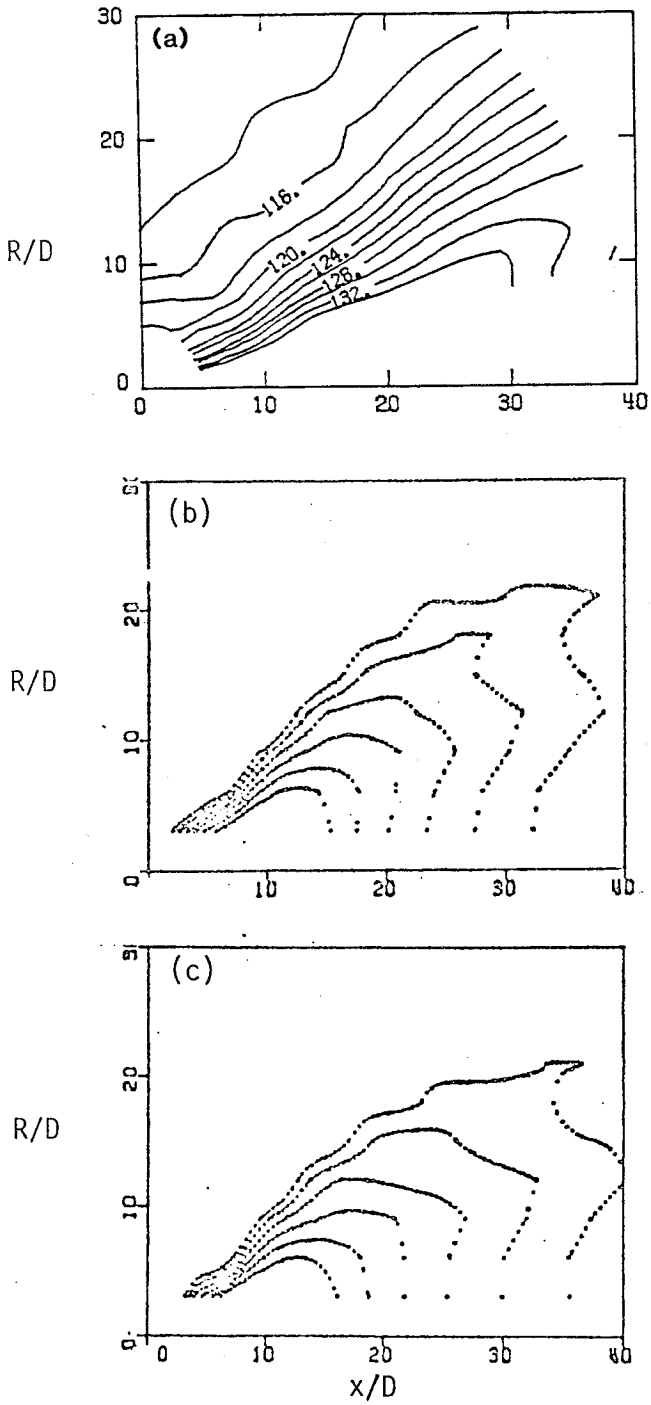

Figure 7. Band Passed Near Field Sound Pressure Level Contours for the St = 0.2 Component of the M = 2.0, Re = 5.2×10^6 Jet

(a) Experiment [Ref. 5]
(b) n = 0 prediction of LSNOIS
(c) n = 0 prediction of LSNOIS } Using Measured Instability Amplitude Evolution

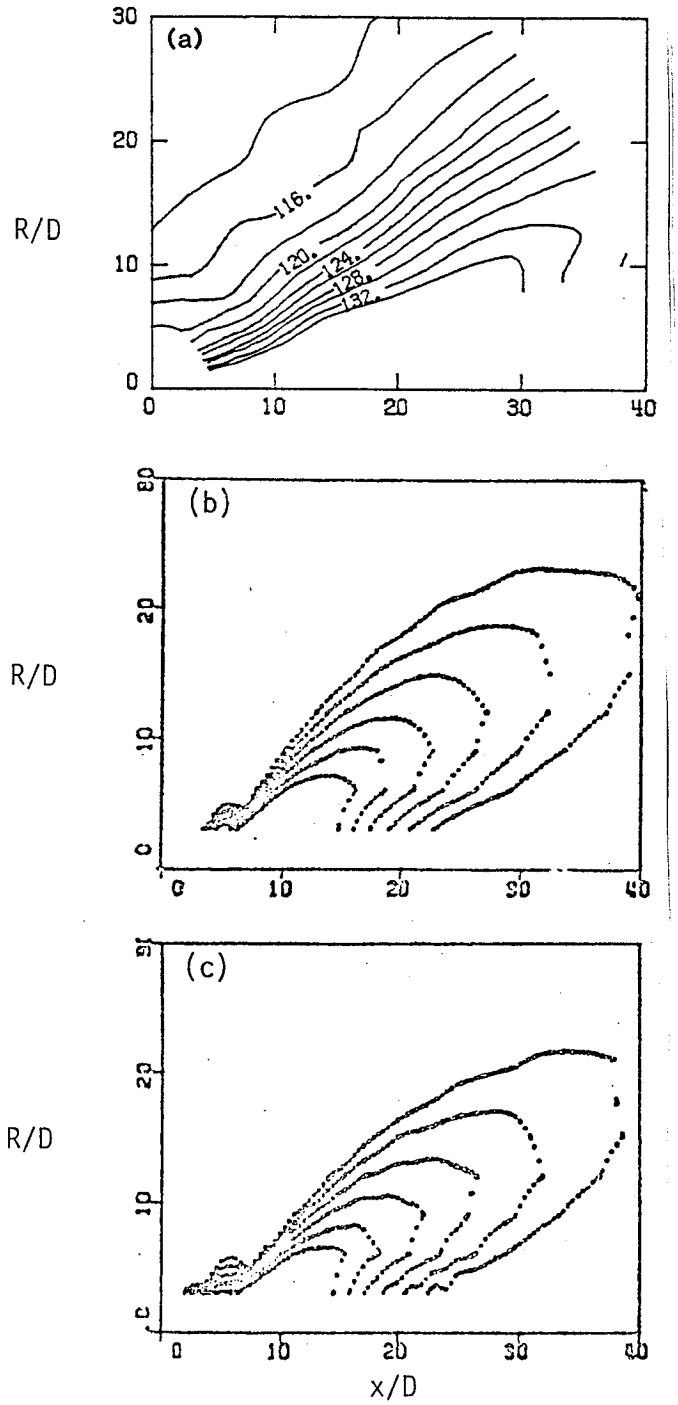

Figure 8. Band Passed Near Field Sound Pressure Level Contours for the St = 0.2 Component of the M = 2.0, Re = 5.2×10^6 Jet

(a) Experiment [Ref. 5]
(b) n = 1 prediction of LSNOIS } Using Measured Instability
(c) n = 1 prediction of LSNOIS } Amplitude Evolution

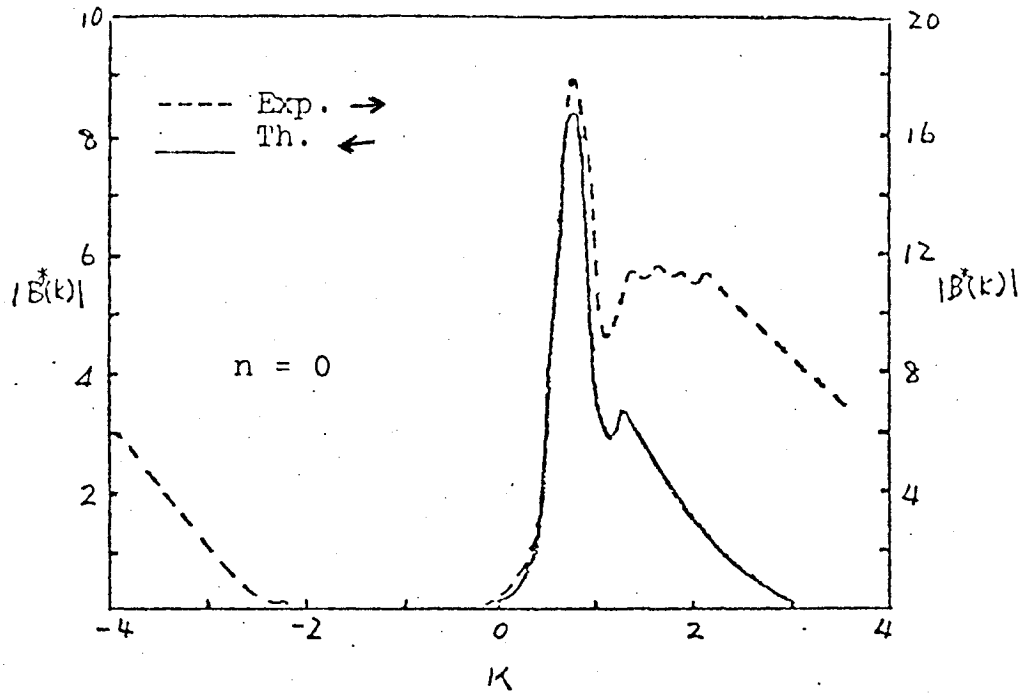

Figure 9. Wavenumber Components of the Experimental and Theoretical Wave Instabilities for the M = 2.0, Re = 5.2×10^6 Jet for the n = 0 mode.

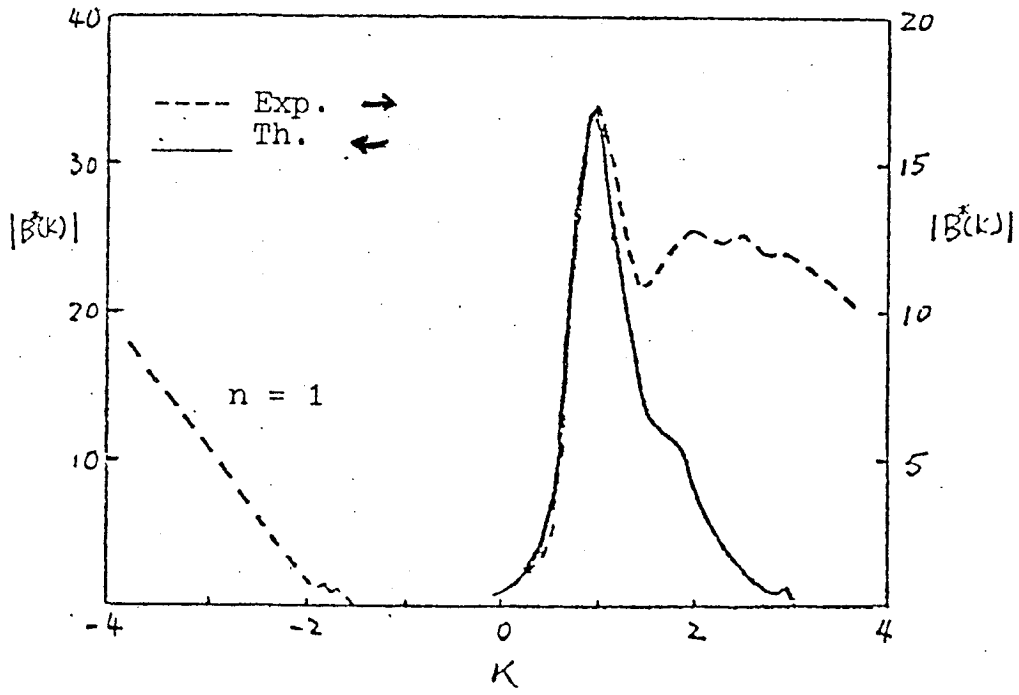

Figure 10. Wavenumber Components of the Experimental and Theoretical Wave Instabilities for the M = 2.0, Re = 5.2×10^6 Jet for the n = 1 mode.

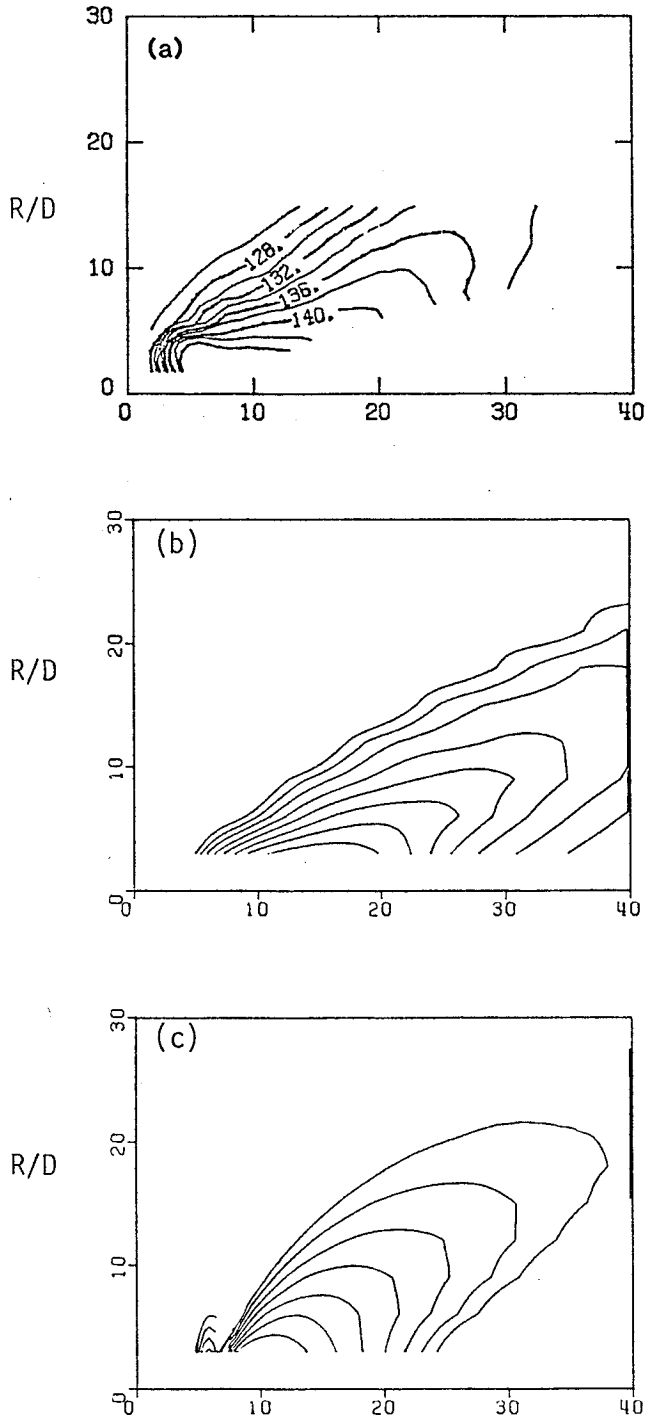

Figure 11. Band Passed Near Field Sound Pressure Level Contours for the St = 0.2 Component of the M = 2.1, Re = 70,000 Jet

(a) Experiment [Ref. 5].

Prediction using measured instability phase and amplitude data: (b) n = 0, (c) n = 1.

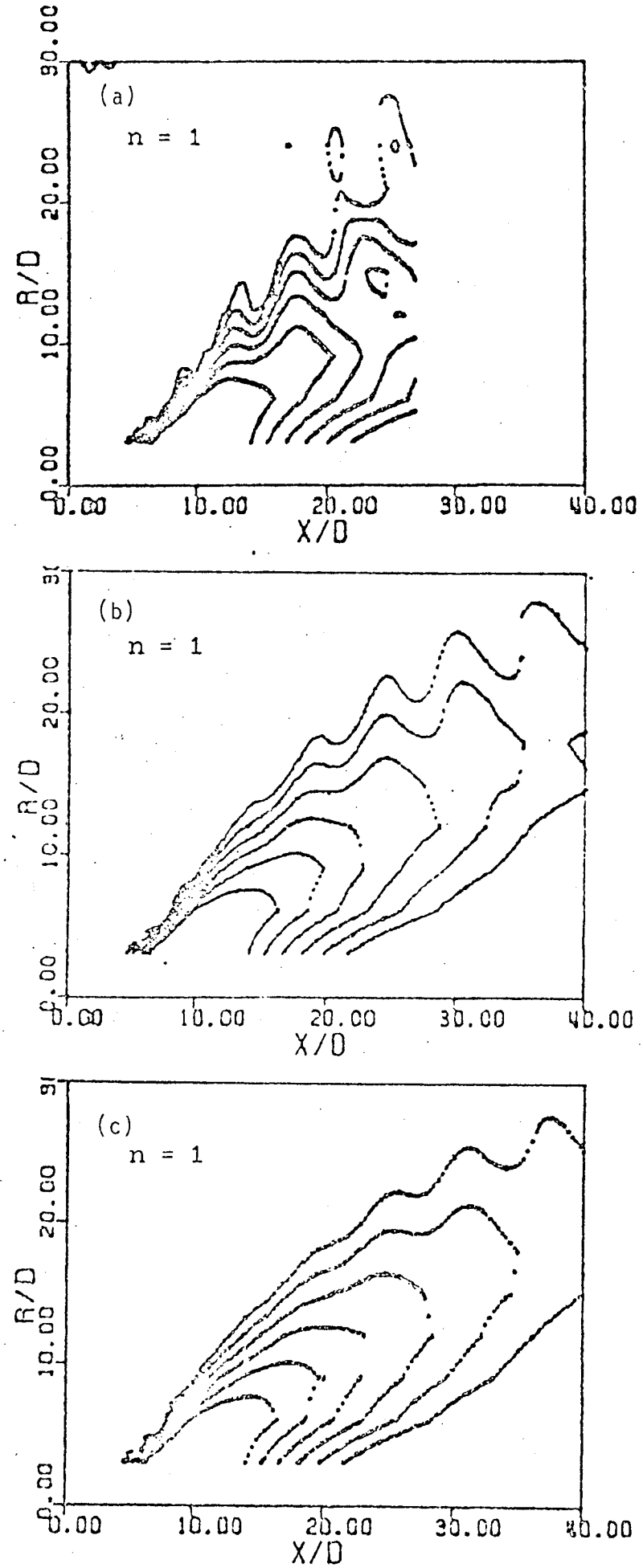

Figure 12.

Predicted Near Field Sound Pressure Level Contours for the St = 0.38 Moderate Reynolds Number Jet Calculated With the Following Step Sizes:

(a) dx = 0.5 DELX
dk = 2.0 DW

(b) dx = DELX
dk = DW

(c) dx = 1.5 DELX
dk = 0.67 DW

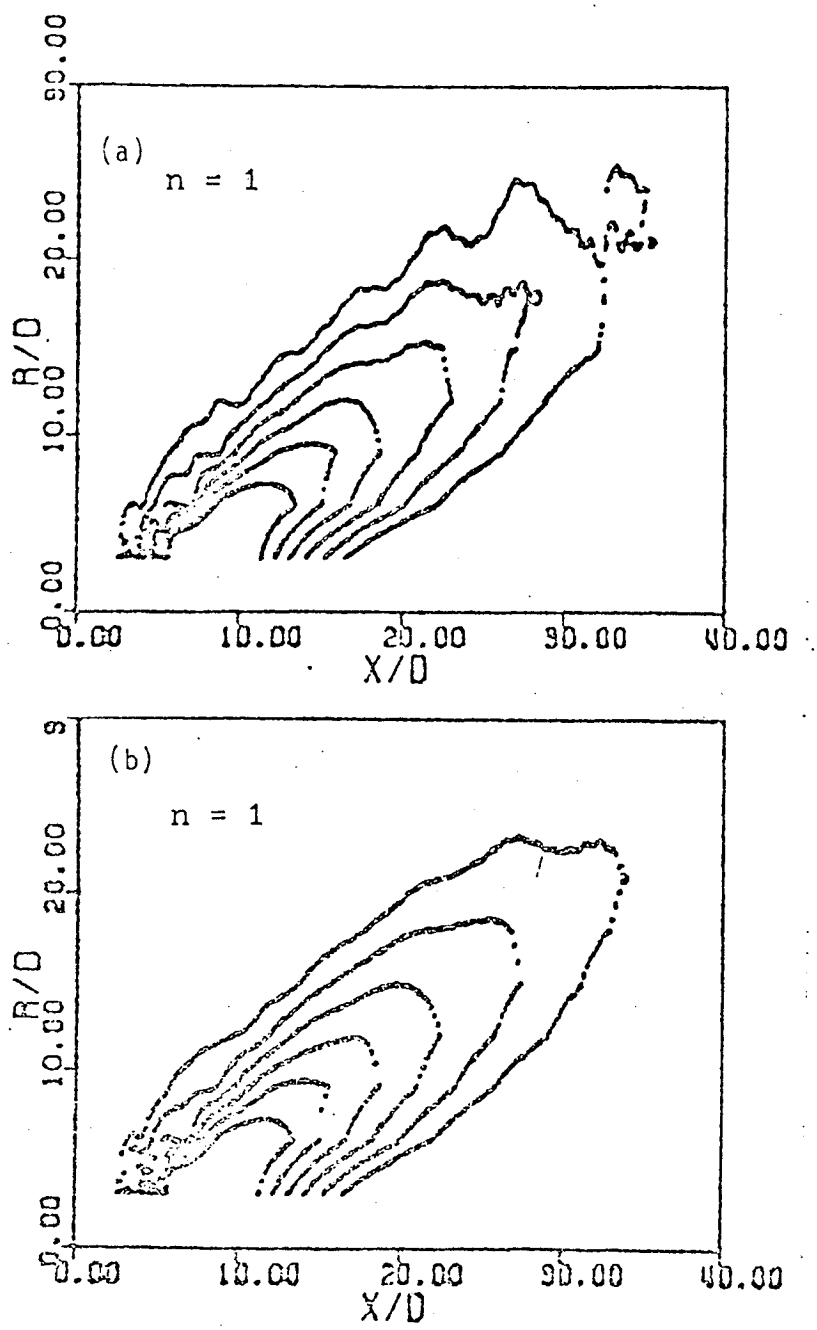

Figure 13. Predicted Near Field Sound Pressure Level Contours Calculated With INUM INcrease and for the St = 0.4 High Reynolds Number Jet. Step Sizes are:

(a) dx = 0.5 DELX
dk = DW

(b) dx = DELX
dk = 0.5 DW